nature communications

Article

https://doi.org/10.1038/s41467-026-71704-5

Maternal antibodies regulate the establishment of murine oral and salivary mucosal immunity

Received: 21 October 2025

Accepted: 25 March 2026

Published online: 10 April 2026

Check for updates

Reem Naamneh[1], Yarin Attar[1], Yasmin Netanely-Rimon[1], Yasmin Jaber[1], Shahd Yacoub[1], Or Saar[2], Olga Georgiev[1], Paz Kles[2], Nadeem Darawshi[1], Reem Bsoul[1], Adina Heinberg[1], Luba Eli-Berchoer[1], Hagit Shapiro[3], Eran Elinav[3,4], Asaf Wilensky[2] & Avi-Hai Hovav[1]

Mucosal homeostasis after birth depends on coordinated interactions between the microbiota and the immune system, with barrier tissues employing distinct mechanisms. Here, we show that maternal Immunoglobulin G (IgG), transferred both in utero and via breastfeeding, reaches the murine neonatal salivary glands and is secreted into saliva, where it recognizes maternal oral microbes and regulates colonization. Offspring lacking in utero-derived IgG show heightened salivary T- and B-cell activation, followed by alterations in the IgG/IgA balance in adult saliva. While postnatal microbiota is essential for priming salivary adaptive immunity, perinatal IgG intrinsically restrains the adaptive responses independent of microbial load. In utero-derived IgG further shapes adult gingival immunity and limits destructive inflammation in murine periodontitis. By contrast, breast milk antibodies promote timely and proper epithelial maturation, a process dependent on microbial load. Thus, we uncover distinct yet complementary roles of pre- and postnatal maternal antibodies in governing oral immune development and long-term protection against oral disease.

Following birth, the oral mucosa is exposed to a surge of microbes, which gradually declines as weaning progresses[1]. Neutrophils, recruited by IL-17-producing γδT cells in a microbiota-dependent manner, protect the neonatal epithelium from bacterial infiltration. During this period, the microbiota promotes epithelial maturation, barrier sealing, and the acquisition of adult immunological functions[1]. Weaning also triggers microbiota-dependent upregulation of the homeostatic regulator GAS6, supporting host-commensal interactions[2]. The microbiota further promotes recruitment of Langerhans cells and γδT cells, which are essential for gingival and epithelial function[3,4]. These findings highlight the dynamic interplay between immune cells and microbiota in establishing oral mucosal homeostasis, though precise mechanisms remain to be fully elucidated.

The salivary system is also crucial for oral mucosal homeostasis. Saliva aids mastication, swallowing, and oral cleansing[5], and shapes the oral microbiota, as many bacteria rely on salivary glycoproteins for growth[6]. Beyond these physiological roles, the saliva contains antimicrobial molecules and complement components that serve as part of the innate defense system[7,8]. Saliva also contains immunoglobulins such as IgA and IgG, which are key mediators of adaptive humoral immunity[9]. Salivary IgA secretion depends on the microbiota and IL-17-producing $CD4^+$ T cells[10]. A recent report further reveals that salivary glands function as immune induction sites, where dendritic cells (DC) migrate from the oral mucosa to activate naïve T cells within the glands[10]. However, whether salivary immunity contributes to the establishment of oral mucosal immunity during the postnatal period remains unclear.

[1]Institute of Biomedical and Oral Research, Faculty of Dental Medicine, Hebrew University, Jerusalem, Israel. [2]Faculty of Dental Medicine, Hebrew University, Jerusalem, Israel; Department of Periodontology, Hadassah Medical Center, Jerusalem, Israel. [3]Department of Systems Immunology, Weizmann Institute of Science, Rehovot, Israel. [4]Microbiome & Cancer Division, DKFZ, Heidelberg, Germany. e-mail: avihaih@ekmd.huji.ac.il

During weaning, adaptive immunity develops in both the oral mucosa and salivary glands, initiating mechanisms that support lifelong mucosal homeostasis[1,10,11]. In contrast, the neonatal immune system is immature and must respond effectively to initial microbial colonization. To protect neonates, maternal IgG is transferred in utero, while both IgA and IgG are delivered through breast milk[12,13]. In the intestine, breast milk-derived IgA and IgG support the development of appropriate anti-commensal responses in the neonatal gut[14,15]. Additionally, IgG protects against enteric pathogens and promotes the establishment of gut homeostasis in early life[16]. Recent work has shown that maternal IgG is actively transported by the neonatal Fc receptor (FcRn) from the circulation to the salivary glands and subsequently secreted into saliva[10]. While this points to a potential protective role for maternal IgG in the oral mucosa, its source, mechanism of action, and long-term impact remain unclear. This study addresses the role of maternal antibody transfer in orchestrating the maturation of oral mucosal immunity after birth. We demonstrate that maternal antibodies acquired both in utero and through breastfeeding play a pivotal role in shaping adaptive immunity in the salivary glands and oral mucosa. The lack of in utero-derived IgG elevates immune activation in the salivary glands and gingiva, alters the load and composition of the oral microbiota, leading to oral dysbiosis and exacerbated experimental periodontitis in adulthood. At the same time, breast milk-derived antibodies influence oral epithelial maturation and impair epithelial integrity. By demonstrating how maternal antibodies protect against oral diseases later in life, our work identifies this immune transfer as a critical window for early-life interventions aimed at programming long-term oral and systemic health.

Results

Maternal IgG antibodies are transferred to the neonatal salivary glands and saliva

To study the influence of maternal antibodies on the development of postnatal immunity in the offspring, a crossbreeding experiment was conducted using $J_HT^{-/-}$ mice, which failed to produce functional B cells as they lack the gene for the heavy chain joining region[17]. $J_HT^{+/+}$ males were crossed with $J_HT^{-/-}$ females to produce offspring with functional B cells but without maternal antibodies (mIg^{neg}). The control group consisted of mating between $J_HT^{-/-}$ males and $J_HT^{+/+}$ females, ensuring functional B cells in the offspring who received maternal antibodies (mIg^{+}) (Fig. 1A). To identify the type of antibodies present in the salivary glands post-birth, we conducted a Western blot and ELISA analysis on the parotid glands of 2-week-old mice. As illustrated in Fig. 1B-C, we observed IgG antibodies in the parotid glands of mIg^{+} offspring, while IgA antibodies were absent. Additionally, IgG antibodies were detectable in the saliva collected from the oral cavity (Fig. 1D) and serum (Fig. 1E) of 3-week-old mIg^{+} but not mIg^{neg} mice. To assess the persistence of maternal IgG in neonatal parotid glands, we crossed $J_HT^{-/+}$ males with $J_HT^{-/+}$ females, and collected homozygous $J_HT^{-/-}$ offspring, which lack B cells, at various time points after birth (Fig. 1F). High levels of maternal IgG were detected in both the salivary glands (Fig. 1F) and serum (Fig. 1G) shortly after birth. These levels declined significantly during weaning but remained detectable up to four weeks postnatally. IgA antibodies were not detectable in the salivary glands of $J_HT^{-/-}$ offspring at any tested time point (Supplementary Fig. 1A). In addition, $J_HT^{-/-}$ offspring born to $J_HT^{-/+}$ dams exhibited no B cells in their parotid glands, suggesting that B cells are not maternally transferred to the offspring (Supplementary Fig. 1B). To assess the contribution of in utero- and breastfeeding-derived IgG to the salivary glands, we conducted a fostering experiment in which the dams of mIg^{+} and mIg^{neg} offspring were exchanged after birth. As shown in Supplementary Fig. 1C, low but detectable levels of in utero-derived IgG were present in 3-week-old fostered mIg^{+} offspring, while higher levels were detected in fostered mIg^{neg} offspring, indicating that IgG from both in utero transfer and breast milk reaches the neonatal salivary glands. We then examined whether the levels of IgG and IgA antibodies in weaned mIg^{+} ($J_HT^{-/+}$) offspring reflect those found in wild-type (WT) mice. Analysis of the parotid gland and saliva revealed comparable IgG levels, whereas IgA was undetectable in both groups, indicating that the two groups exhibit similar salivary antibody isotype profiles (Supplementary Fig. 1D). Next, we examined the presence of maternal antibodies in the parotid glands of 4-week-old WT mice under specific pathogen-free (SPF) and germ-free (GF) conditions. IgG antibodies were detected exclusively in SPF mice, whereas IgA antibodies were absent in both groups (Fig. 1H and Supplementary Fig. 1E). These findings suggest that during neonatal life, the salivary glands and saliva contain substantial levels of maternal IgG antibodies derived from both in utero transfer and breastfeeding. In addition, since GF mice harbor reduced IgG levels[18], while FcRn expression remains intact postnatally[10], the lack of IgG in GF offspring is likely attributable to the limited availability of maternal antibodies for transfer, rather than to a defect in FcRn-mediated translocation.

Absence of in utero-derived maternal IgG drives elevated adaptive immunity in early-life salivary glands

To examine the influence of maternal IgG on the development of adaptive immunity in the salivary glands, mIg^{+} and mIg^{neg} mice were analyzed at four weeks of age, a time point that coincides with weaning and the onset of adaptive immune development in these glands[10]. As illustrated in Fig. 2A and Supplementary Fig. 2A, B, flow cytometry analysis indicated that while the frequencies and numbers of total $CD45^{+}$ leukocytes were not changed, the frequencies and counts of $CD4^{+}$ T cells, $CD8^{+}$ T cells, and B cells were significantly elevated in the mIg^{neg} offspring. Notably, the $Ly6C^{+}$ $CD4^{+}$ and $CD8^{+}$ T cells, representing short-lived activated T cells (DeLong et al., 2018), were also increased in mice lacking maternal antibodies. In contrast, mIg^{neg} offspring display reduced frequencies and numbers of macrophages (Fig. 2A and Supplementary Fig. 2A, B). To determine the origin of maternal antibodies shaping adaptive immunity in the salivary glands, we conducted a fostering experiment in which dams were swapped between experimental groups after birth, and the offspring were assessed four weeks later. As illustrated in Fig. 2B, increased frequencies and numbers of B cells were observed in the salivary glands of offspring that did not receive maternal antibodies in utero, regardless of whether they received maternal antibodies through breast milk. Additionally, higher frequencies and numbers of T cells were detected in offspring that received maternal antibodies in utero compared to those that did not (Fig. 2B). Notably, fostered offspring exhibited an overall elevation in the T cells compared to the unfostered control group, suggesting that the fostering process may enhance cell-mediated immunity in these mice. To further investigate the impact of maternal antibodies on salivary immunity, we examined the ability of oral DCs to migrate to the salivary glands, given their reported role in priming T cells in this context[10]. First, as depicted in Supplementary Fig. 2C, DCs (both $CD11b^{+}$ and $CD103^{+}$ DC subsets) were present in the oral mucosa of 3-week-old mice, while Langerhans cells, the APCs of the epithelium, were not yet developed. Subsequently, we applied FITC solution to the oral mucosa of 3-week-old mice and, three days later, quantified the frequencies of FITC-labeled cells in the salivary glands, indicative of migratory DCs. Upon gating on $MHCII^{+}CD11c^{+}B220^{neg}$ cells, representing DCs and macrophages, and further on $CD11c^{+}CD64^{neg}$ (DCs) and $CD64^{+}$ (macrophages) cells, higher frequencies of $FITC^{+}$ DCs were found in mIg^{neg} offspring compared to mIg^{+} mice (Fig. 2C). In fact, the frequencies of DCs among the total APCs were elevated in the salivary glands due to the absence of maternal antibodies (Fig. 2D). Moreover, increased production of IFN-γ was observed by $CD4^{+}$ and $CD8^{+}$ T cells of the mIg^{neg} group, whereas IL-17 production was not detected (Fig. 2E). Consistently, $CD4^{+}$ T cells from mIg^{neg} offspring exhibited elevated expression of the early activation marker CD69 (Fig. 2F), along with a reduced frequency of $FOXP3^{+}$ $CD4^{+}$ regulatory T cells (Tregs) (Fig. 2G). It is worth mentioning that at this early age, the salivary glands contain $CD11b^{+}$ DCs and $CD103^{+}$ DCs (Supplementary Fig. 2D). The former expresses CD301a, which has been

https://doi.org/10.1038/s41467-026-71704-5

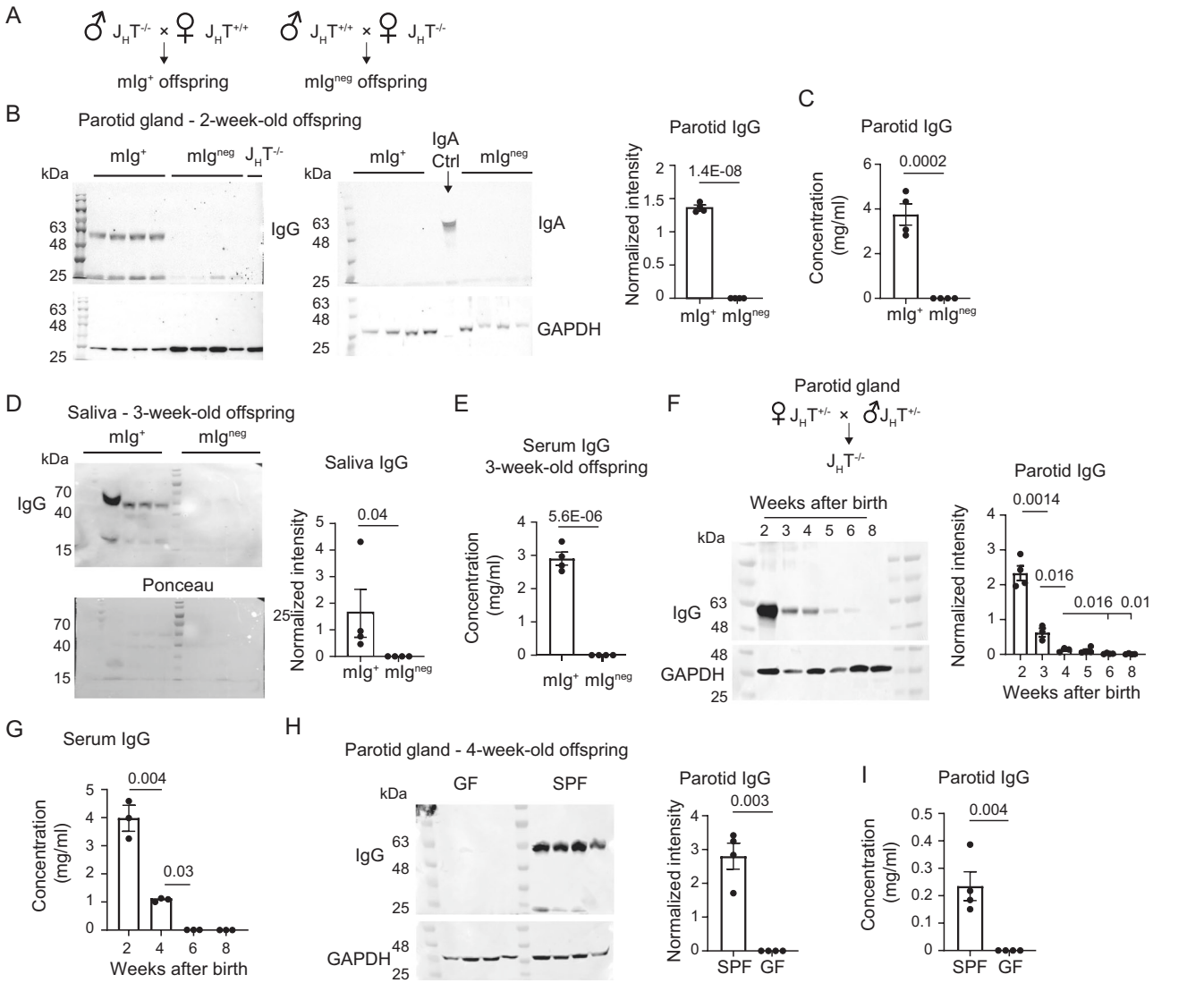

Fig. 1 | Maternal IgG antibodies are transferred to the neonatal salivary glands and saliva. A $J_HT^{+/+}$ males were crossed with $J_HT^{-/-}$ females, or $J_HT^{-/-}$ males were crossed with $J_HT^{+/+}$ females, to generate mIg^{neg} and mIg^{+} mice, respectively. **B** Western blot analysis of IgG and IgA in parotid glands of 2-week-old mIg^{+} and mIg^{neg} mice; GAPDH served as a loading control. Serum IgA from adult WT mice was used as a positive control. The graph shows IgG levels ± SEM normalized to GAPDH ($n = 4$). Representative of five independent experiments. **C** Mean IgG concentration ± SEM in parotid glands of 2-week-old mIg^{+} and mIg^{neg} mice measured by ELISA ($n = 4$). Representative data from two independent experiments. **D** Western blot detection of IgG in the saliva of 3-week-old mIg^{+} and mIg^{-} mice. Quantification (±SEM) was normalized to total salivary protein by Ponceau staining ($n = 4$). Representative data of two independent experiments. **E** Mean serum IgG concentration ±SEM in 3-week-old mIg^{+} and mIg^{neg} mice measured by ELISA ($n = 4$). Representative data from two independent experiments. **F** Western blot detection of IgG in parotid glands of $J_HT^{-/-}$ offspring born to B-cell–intact hemizygous ($J_HT^{-/+}$) parents at the indicated weeks after birth. GAPDH served as a control. Quantification shows IgG levels ±SEM normalized to GAPDH and referenced to 2-week levels ($n = 3$ for weeks 2-4; $n = 4$ for weeks 5–8). Representative data of three independent experiments. **G** Mean serum IgG concentration ± SEM at indicated postnatal weeks in $J_HT^{-/-}$ offspring born to $J_HT^{-/+}$ parents measured by ELISA ($n = 3$). Representative data from two independent experiments. **H** Western blot detection of IgG in parotid glands of 4-week-old GF and SPF WT mice; GAPDH served as a control. Quantification shows IgG ±SEM normalized to GAPDH ($n = 4$). Representative data from two independent experiments. **I** Mean parotid IgG concentration ±SEM in 4-week-old SPF and GF mice measured by ELISA ($n = 4$). Representative data from two independent experiments. Statistical analysis: *p*-value from a two-tailed, unpaired t-test and an ordinary one-way ANOVA test using GraphPad Prism.

shown to present commensal antigens for generating Treg cells in neonatal life[19]. In conclusion, these results demonstrate that maternal IgG antibodies transferred in utero are essential for downregulating adaptive immunity in the salivary glands of offspring during early life.

Maternal IgG recognizes the maternal oral microbiota, enhances phagocytosis, prevents epithelial adhesion, and delays the expression of adult epithelial markers

Maternal IgG antibodies shape the neonatal microbiota and support intestinal homeostasis[14,16], while also protecting against pathogens[20]. Given that the microbiota plays a crucial role in shaping oral immunity during early life[1], we sought to investigate whether maternal IgG antibodies affect the neonatal oral microbiota. We first assessed whether these antibodies recognize the oral microbiota by performing an ELISA on serum from SPF and GF neonates using microbiota samples from various sources. As illustrated in Fig. 3A, the serum from SPF neonates exhibited strong recognition of the oral microbiota derived from their mothers, surpassing the recognition levels observed when exposed to oral microbiota from unrelated mothers. The serum from GF neonates displayed no recognition of the microbiota. Maternal IgG antibodies from SPF neonates also recognized the intestinal microbiota collected from their mothers (Fig. 3A). The subtypes of maternal

https://doi.org/10.1038/s41467-026-71704-5

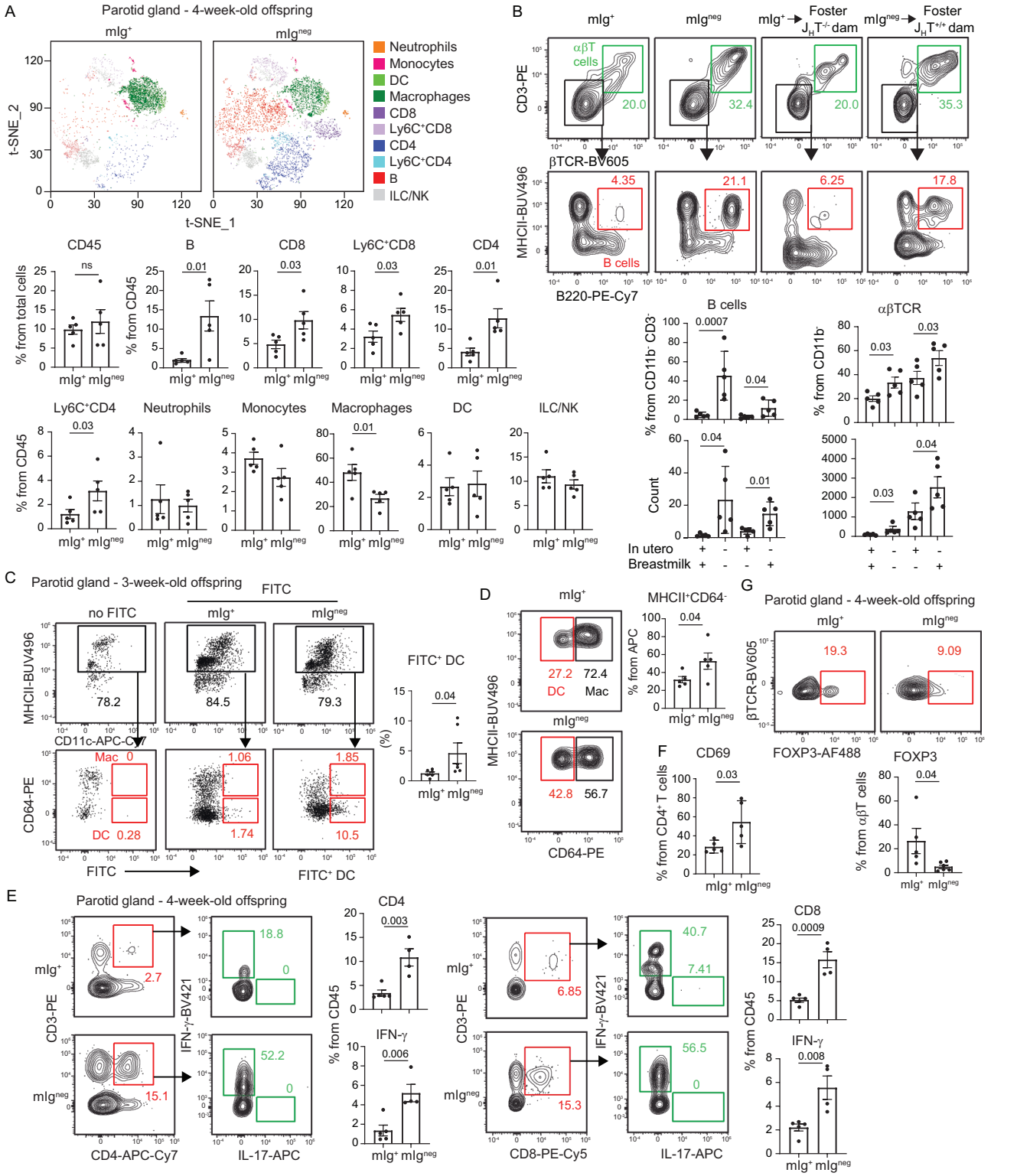

Fig. 2 | In utero delivered maternal IgG antibodies regulate salivary gland adaptive immunity. A t-SNE flow cytometry plots display the main subsets of leukocytes present in the parotid glands of 4-week-old mIg$^+$ and mIg^{neg} mice. Graphs show the mean frequencies ± SEM ($n = 5$) of the various leukocytes in the parotid glands of each group. DC, dendritic cells; ILC, innate lymphoid cells; NK, natural killer cells. Data from one out of four independent experiments are shown. **B** Representative flow cytometry plots and graphs present the mean frequencies ± SEM ($n = 5$) of CD4$^+$ T cells and B cells in the parotid gland of mice cross-fostered with $J_HT^{-/-}$ or $J_HT^{+/+}$ dams after birth. Representative data from two independent experiments. **C** The oral cavity of mIg$^+$ and mIg^{neg} mice was painted with FITC solution, and 3 days later, the parotid glands were analyzed. Flow cytometry plots and a graph present the mean frequencies ± SEM ($n = 6$) of FITC-labeled DCs. Representative data of two independent experiments. **D** Representative flow cytometry plots and graphs present the mean frequencies ± SEM of DCs ($n = 5$) in the parotid glands of 4-week-old mIg$^+$ and mIg^{neg} mice. Representative data of two independent experiments. **E**–**G** The mean frequencies ± SEM (mIg$^+$ $n = 4$; mIg^{neg} $n = 4$ and 6) of IFN-γ, IL-17A, CD69, and FOXP3 expressing CD4$^+$ or CD8$^+$ T cells in the parotid glands of 4-week-old mIg$^+$ and mIg^{neg} mice. Representative data of three independent experiments. Statistical analysis: *p*-value from a two-tailed, unpaired t-test and an ordinary one-way ANOVA test.

https://doi.org/10.1038/s41467-026-71704-5

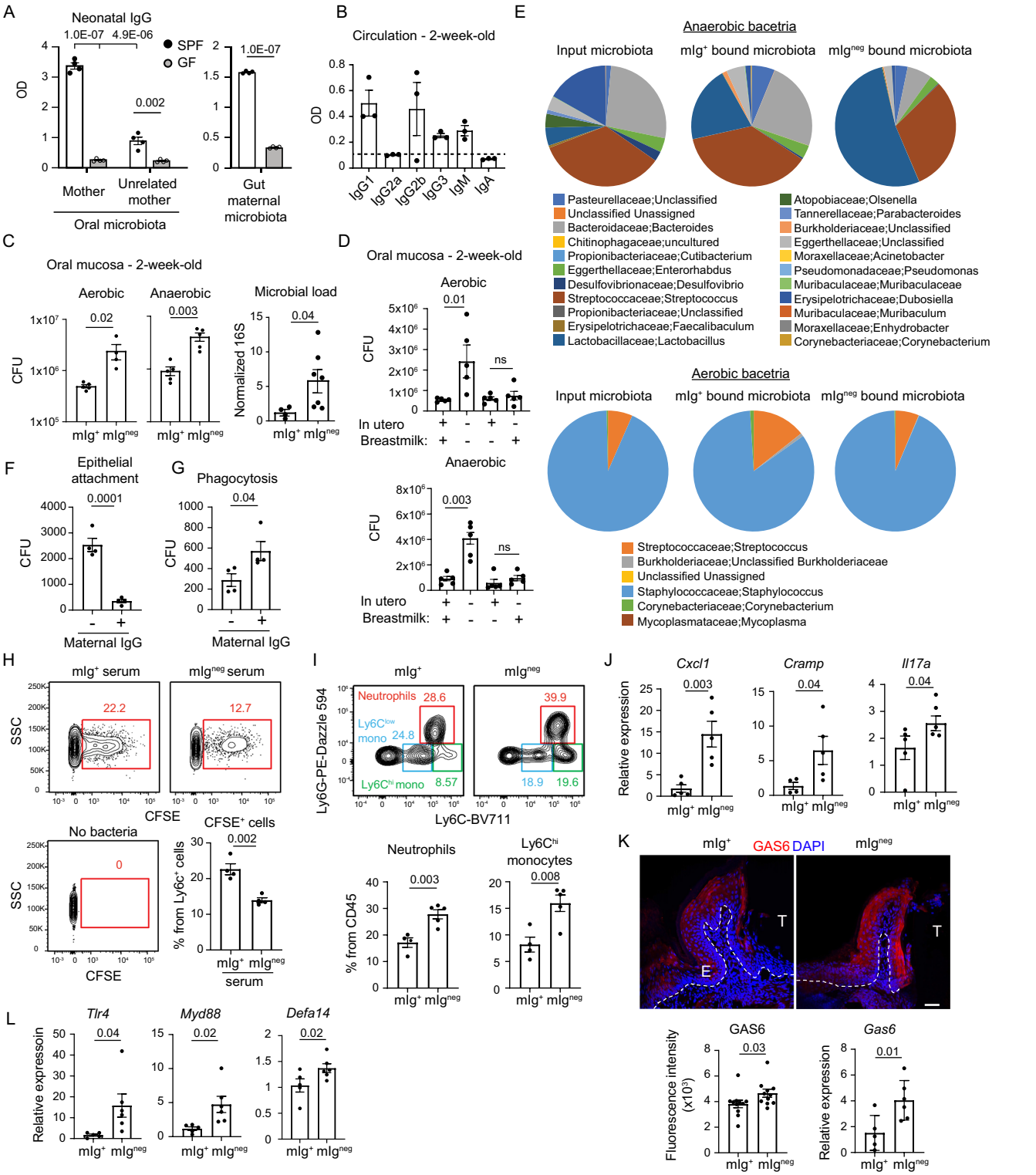

IgG antibodies were then examined in the serum of 2-week-old offspring, revealing the presence of IgG1, IgG2b, and IgG3 antibodies (Fig. 3B). IgM was also detected in the neonatal serum, while IgA antibodies were undetectable, similar to IgG2a, a subtype that is not generated by B6 mice. Analysis of IgG subtypes in the parotid glands and saliva of 2-week-old offspring revealed the presence of all IgG isotypes, with IgG2b being the most abundant in the glands and saliva (Supplementary Fig. 3A). Among these isotypes, IgG2b demonstrated the highest affinity for the maternal oral microbiota, with IgG1 showing moderate binding (Supplementary Fig. 3B). Next, the oral microbial load of mIg^{+} and mIg^{neg} neonates was quantified, revealing a higher load of cultivated aerobic and anaerobic bacteria, as well as elevated bacterial ribosomal 16S DNA, in the absence of maternal antibodies (Fig. 3C). To determine the origin of maternal antibodies that regulate the oral microbiota in early life, a fostering experiment was conducted. As shown in Fig. 3D, oral microbial levels were reduced in both fostered groups, with no significant differences between them, indicating that antibodies transferred via both the placenta and breast milk contribute to this effect. Notably, in addition to the presence of breast milk-derived IgG in the salivary system (Supplementary Fig. 1C), breast milk

Fig. 3 | Maternal antibodies reduce the neonatal oral microbial load and delay the acquisition of adult features of the gingival epithelium. A Mean binding levels±SEM ($n = 4$) of circulating neonatal IgG from SPF and GF mice to microbiota from the indicated sources measured by ELISA. Representative of three experiments. **B** Mean levels±SEM ($n = 3$) of circulating antibody subtypes in 2-week-old mice. The dotted line indicates the background without serum. Representative of three experiments. **C** Oral microbiota in 2-week-old mIg$^+$ and mIg^{neg} mice quantified by aerobic and anaerobic CFU counts (mIg$^+$ $n = 5$; mIg^{neg} $n = 4$–5) and by 16S qPCR (mIg$^+$ $n = 4$; mIg^{neg} $n = 7$). Representative of two experiments. **D** CFU ± SEM ($n = 5$) of aerobic and anaerobic oral microbiota in 2-week-old cross-fostered mice. Representative of two experiments. **E** IgG-seq analysis of sera from mIg$^+$ and mIg^{neg} neonates for reactivity against cultivated maternal oral bacteria. Pie charts show the relative abundance of antibody-bound taxa compared to the input microbiota. Representative of two experiments. **F** Attachment of maternal oral microbiota to an epithelial cell line after incubation with serum from 2-week-old neonates containing maternal IgG (±SEM, $n = 4$ biological replicates; serum from individual offspring). Representative of two experiments. **G** Phagocytosis of maternal bacteria by RAW264.7 cells following opsonization with neonatal serum (±SEM, $n = 4$ biological replicates). Representative of two experiments. **H** CFSE-labeled maternal microbiota uptake by freshly isolated neutrophils after opsonization with serum from mIg$^+$ and mIg^{neg} neonates (±SEM, $n = 4$ biological replicates). Representative of two experiments. **I** Frequencies±SEM (mIg$^+$ $n = 4$; mIg^{neg} $n = 5$) of neutrophils and Ly6C^{hi} monocytes in the oral mucosa of 2-week-old mIg$^+$ and mIg^{neg} mice. Representative of two experiments. **J** qPCR quantification of *Cxcl1, Il17a, and Cramp* expression in the gingiva (mean ± SEM, $n = 5$). Representative of two experiments. **K** Immunofluorescence of gingival sections stained for GAS6 and DAPI. Graphs show MFI ± SEM ($n = 11$ sections/4 mice) and Gas6 mRNA levels ± SEM (mIg$^+$ $n = 5$; mIg^{neg} $n = 6$). Scale bar, 50 µm. Representative of two experiments. The dotted line signifies the basal membrane. E, epithelium, T, tooth. **L** Relative expression of indicated genes in oral mucosa by qPCR (mean ± SEM, mIg$^+$ $n = 5$; mIg^{neg} $n = 6$). Representative of two experiments. *p*-value from a two-tailed, unpaired t-test and an ordinary one-way ANOVA test.

IgA was also detected in the saliva of WT neonates, albeit at very low levels, as salivary IgG exceeded IgA by roughly three orders of magnitude (Supplementary Fig. 3C), suggesting that IgA is unlikely to play a significant role in shaping the neonatal oral microbiota. To identify oral maternal bacteria recognized by maternal IgG, we performed IgG-seq analysis with modifications. Because the sampled oral microbiota was too sparse for direct analysis, maternal oral samples were first plated under aerobic and anaerobic conditions, and the cultivated bacteria were subjected to IgG-seq using serum from 2-week-old mIg$^+$ and mIg^{neg} offspring. As demonstrated in Fig. 3E, anaerobic bacterial families that were over-represented upon incubation with mIg$^+$ serum compared to the input microbiota (the total cultivated oral microbiota) consist of *Pasteurellaceae, Burkholderiaceae*, and *Corynebacteriaceae*. Additionally, although *Bacteroidaceae* and *Muribaculaceae* were not enriched relative to the input microbiota, their abundance was higher than that observed after incubation with serum from mIg^{neg} offspring, suggesting lower affinity binding by maternal IgG. Within the aerobic bacteria, the families *Mycoplasmataceae*, *Betaproteobacteriales*, and *Corynebacteriaceae* were over-represented compared to the input microbiota (Fig. 3E). We further assessed the functional role of maternal IgG and found that it inhibited bacterial attachment to oral epithelial cells (Fig. 3F) and enhanced phagocytosis by RAW264.7 cells or freshly isolated neutrophils (Fig. 3G, H). These findings suggest that maternal IgG recognizes specific maternal oral microbial taxa and can limit their epithelial adhesion while promoting clearance via phagocytosis postnatally.

Next, we investigated whether the elevated oral microbial load detected in mIg^{neg} neonates impacts gingival immunity. Flow cytometry analysis revealed increased frequencies of neutrophils and inflammatory Ly6C^{hi} monocytes in the oral mucosa of 2-week-old mIg^{neg} mice compared to mIg$^+$ mice (Fig. 3I). Consistently, elevated mRNA levels of *Cxcl1* and *Il17a*, both involved in neutrophil recruitment, as well as *Cramp*, which is expressed by neutrophils, were detected in the oral tissues of mIg^{neg} mice (Fig. 3J). To determine whether the neonatal oral epithelium is permeable to IgG antibodies, allowing them to opsonize bacteria for phagocytosis by intraepithelial neutrophils, we applied anti-CD45 IgG antibodies to the oral epithelium of 1- and 8-week-old mice. Positive staining of CD45-positive cells was observed in 1-week-old mice, whereas reduced staining was observed in 8-week-old mice (Supplementary Fig. 4A). Western blot analysis and immunofluorescence staining confirmed the presence of maternal IgG antibodies in the neonatal oral epithelium (Supplementary Fig. 4B, C). Next, the expression level of GAS6, a key immunological factor upregulated during weaning and signifying the transition of the neonatal oral epithelium to an adult phenotype, was examined[2]. GAS6 expression was significantly elevated at both the RNA and protein levels in the gingiva of 2-week-old mIg^{neg} mice compared to the mIg$^+$ control group (Fig. 3K). Consistently, the levels of *Tlr4*, Myd88, and *Defa14*, genes associated with postnatal maturation of the oral epithelium[1], were also upregulated in the mIg^{neg} mice (Fig. 3L). Collectively, these findings indicate that maternal IgG antibodies, acquired both in utero and through breastfeeding, recognize maternal oral bacteria and can restrict their epithelial adherence, promote phagocytic clearance, and modulate gingival immune responses and epithelial development during early life.

Maternal IgG antibodies modulate structural, functional, and immunological parameters of the salivary glands

To gain further insight into the impact of maternal antibodies on the salivary glands, we conducted a comprehensive analysis of global gene expression in the parotid glands of mIg$^+$ and mIg^{neg} offspring 4 weeks after birth. Hierarchical clustering (Fig. 4A) and principal component analysis (PCA) (Fig. 4B) demonstrated a significant distinction between the transcriptomic profiles of the two groups. Gene set enrichment analysis (GSEA) revealed that cellular pathways associated with cell growth and differentiation, such as the EF2 target, G2M checkpoint, mitotic spindle, MYC targets, and KRAS signaling, were upregulated in the mIg^{neg} group[21] (Fig. 4C). Additionally, pathways involved in tissue regeneration, including epithelial-mesenchymal transition, myogenesis, and angiogenesis[22,23], were found to be increased. Conversely, pathways related to metabolism, such as oxidative phosphorylation, glycolysis, protein secretion, heme metabolism, fatty acid metabolism, xenobiotic metabolism, and adipogenesis[24,25], were downregulated in the mIg^{neg} group. Many of these pathways are known to be regulated by P53 and TGF-β, which were also downregulated in the mIg^{neg} offspring[26,27]. Moreover, IFN-α-associated responses, a cytokine known to induce hypoactivation of the salivary glands upon immune activation[28], were reduced in the mIg^{neg} group. Given the altered transcriptomic signature observed in the parotid glands of mIg$^+$ and mIg^{neg} offspring, indicating potential structural and functional changes, we conducted further investigations. As illustrated in Fig. 4D, histological cross-sections of the parotid glands revealed higher numbers of excretory ducts in mIg^{neg} offspring compared to mIg$^+$. Moreover, the saliva flow generated by the salivary glands was higher in the mIg^{neg} offspring (Fig. 4E). Together, these findings indicate that maternal antibodies modulate the structural and functional characteristics of the salivary glands.

Next, since maternal antibodies are directed against the microbiota, we asked if they regulate the microbial load in the salivary glands and whether the microbiota affects local immunity. First, using fluorescence in situ hybridization (FISH) for visualization of bacterial 16S rRNA, heightened bacterial load was observed in the parotid glands of 2-week-old neonatal mIg^{neg} mice (Fig. 4F). Next, the leukocytes of the salivary glands were examined in GF and SPF mice 4 weeks after birth using flow cytometry. As demonstrated in Fig. 4G, H, the parotid glands of GF mice contained substantially reduced

https://doi.org/10.1038/s41467-026-71704-5

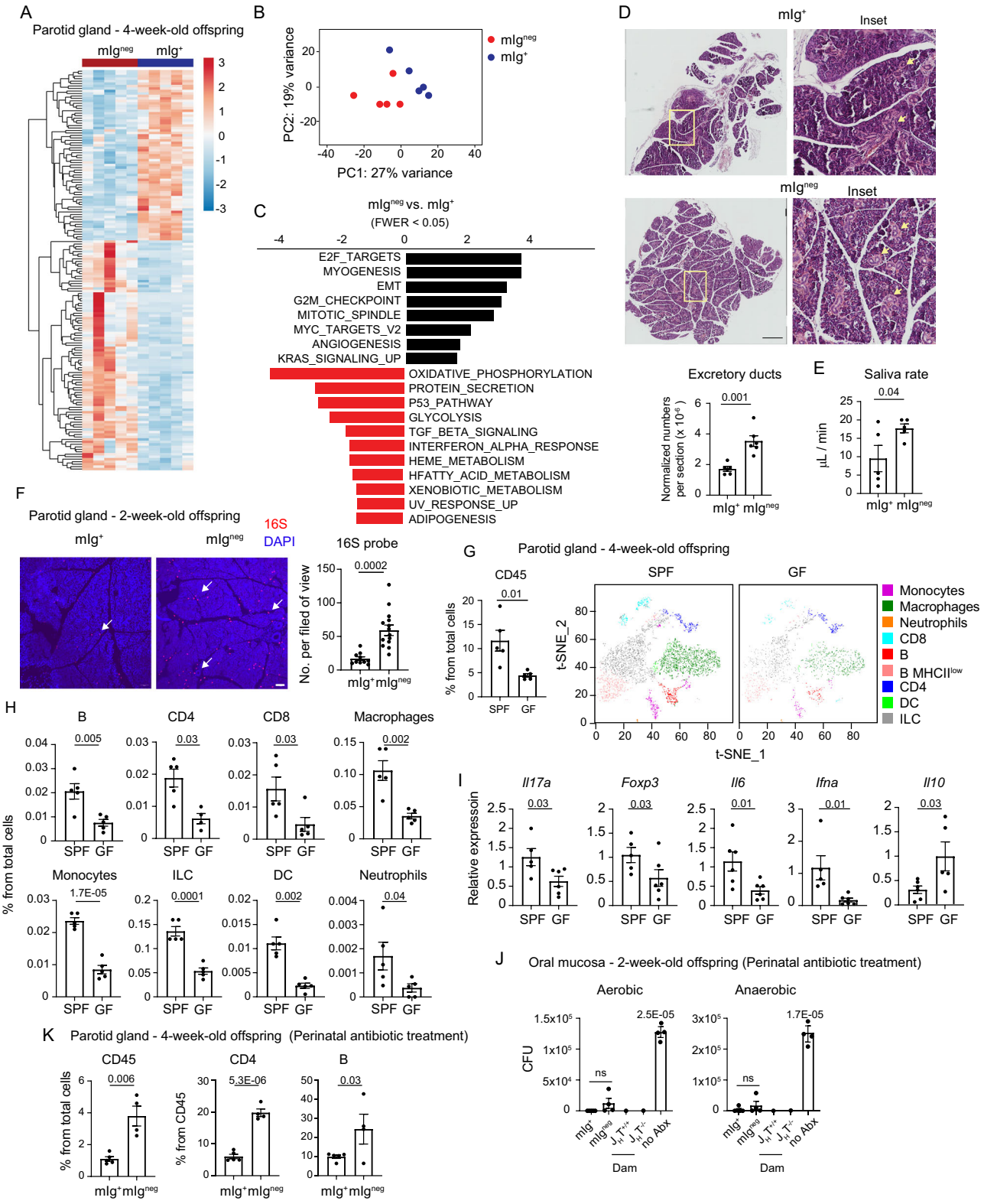

frequencies of total leukocytes, affecting all types of immune cells. Consistent with this finding, the expression of key immunological genes such as *Il17a*, *Foxp3*, *Il6*, and *Ifna* was reduced in the GF parotid gland, except for *Il10*, which was upregulated (Fig. 4I). To determine whether the capability of maternal antibodies to modulate mucosal immune responses is affected by the bacterial load, we administered broad-spectrum antibiotics to pregnant dams and their offspring until weaning. As shown in Fig. 4J, perinatal antibiotic treatment reduced the early-life oral bacterial burden in both mothers and pups, allowing a comparison of immune responses under comparable microbial load. Despite similarly reduced bacterial loads, flow cytometry analysis of the salivary glands in 4-week-old offspring revealed increased frequencies of CD4$^+$ T cells and B cells in the mIg^{neg} group compared to the mIg$^+$ group (Fig. 4K). These findings suggest that although the microbiota is required to initiate salivary adaptive immunity, maternal IgG antibodies modulate this response through a distinct immunoregulatory mechanism that is not affected by the microbial load.

Fig. 4 | Maternal IgG antibodies modulate structural and functional features of the salivary glands. A Hierarchical clustering of the genes differentially expressed in the parotid glands of 4-week-old mIg$^+$ and mIg^{neg} mice. **B** PCA of the most variable transcripts expressed by the different parotid gland cells. **C** GSEA identifies significantly upregulated and downregulated pathways in mIg$^+$ versus mIg$^-$ parotid glands (FWER < 0.05). **D** Representative H&E staining of parotid gland cross-sections from 4-week-old mIg$^+$ and mIg$^-$ mice. Yellow arrows indicate excretory ducts. Scale bar, 100 µm. Bar graph shows mean duct numbers ± SEM normalized to gland area (n = 6 sections from 3 mice). Representative of two experiments. **E** Saliva production rates in 8-week-old mIg$^+$ and mIg$^-$ mice are shown as mean ± SEM ($n = 5$). Representative of two experiments. **F** Detection of bacterial 16S rRNA by fluorescence in situ hybridization (red) with DAPI counterstain (blue) in parotid sections of 2-week-old mice. Yellow arrows indicate labeled bacteria. Quantification shows mean 16S signal per field ± SEM (mIg$^+$ $n = 10$ sections from 4–5 mice; mIg$^-$ $n = 14$ sections from 5 mice). Representative of two experiments. Scale bar, 25 µm. **G** Mean frequencies ± SEM ($n = 5$ mice) of CD45$^+$ leukocytes in parotid glands of 4-week-old SPF and GF mice, with t-SNE plots illustrating major immune populations. **H** Frequencies ± SEM ($n = 5$) of principal leukocyte subsets in SPF and GF parotid glands. Representative of two experiments. **I** Relative expression of selected immune genes in parotid glands of 4-week-old SPF and GF mice measured by qPCR and normalized to SPF controls (SPF $n = 5$; GF $n = 6$; mean ± SEM). Representative of two experiments. **J** Mean CFU ± SEM ($n = 4$) of aerobic and anaerobic oral bacteria in 2-week-old offspring and their mothers following broad-spectrum antibiotic treatment during gestation and postnatally. Representative of two experiments. (**K**) Frequencies ± SEM ($n = 4$) of total leukocytes, CD4$^+$ T cells, and B cells in parotid glands of antibiotic-treated offspring assessed by flow cytometry. Representative of two experiments. Statistical analysis: *p*-value from a two-tailed, unpaired t-test and an ordinary one-way ANOVA test.

Offspring lacking maternal antibodies exhibit altered salivary immunity in adulthood

Next, we evaluated the impact of maternal antibody deficiency on salivary immunity in adult offspring. Flow cytometry analysis of 8-week-old mice showed similar frequencies of CD4$^+$ T cells and B cells in both mIg^{neg} and mIg$^+$ groups (Fig. 5A). However, the antibody secretion profile differed, as mIg^{neg} mice displayed higher IgG and lower IgA levels compared to mIg$^+$ mice (Fig. 5B, C). Unlike CD4$^+$ T cells, CD8$^+$ T cell frequencies were elevated in the adult mIg^{neg} group (Fig. 5A), accompanied by an increased neutrophil population (Fig. 5D). Microbiota analysis via FISH targeting bacterial 16S rRNA revealed higher bacterial loads in mIg^{neg} mice (Fig. 5E). These findings suggest that the absence of maternal antibodies disrupts salivary B-cell antibody production also in adulthood. Furthermore, the microbiota of adult salivary glands increased in the absence of maternal antibodies, correlating with higher frequencies of neutrophils and CD8$^+$ T cells.

In utero-derived maternal IgG antibodies regulate the development of oral microbial and immunological homeostasis in adult life

The impact of maternal antibodies on the adult salivary glands led us to examine whether oral mucosal homeostasis is also affected in adulthood. To test the oral microbiota, the oral cavity was sampled from 8-week-old mIg^{neg} and mIg$^+$ mice and subjected to taxonomic analysis. First, we quantified the bacterial load and found higher cultivated aerobic and anaerobic bacteria in mIg^{neg} mice than in mIg$^+$ mice (Fig. 6A). Second, alpha diversity analysis revealed higher taxa richness in mIg^{neg} mice compared with mIg$^+$ mice (Fig. 6B). Furthermore, the composition of taxa differed significantly between these groups, as demonstrated by PCA (Fig. 6C). Heat tree analysis further reveals an increased abundance of *Proteobacteria*, typically associated with inflammation, relative to *Firmicutes* in mIg^{neg} mice (Fig. 6D). A single-factor analysis identified a significant expansion of the *Pasteurellaceae* family, which includes opportunistic oral pathogens, alongside a reduction of the *Enterococcaceae* family, which contains commensal species known to contribute to mucosal health (Fig. 6E). To determine the source of maternal antibodies that regulate the adult oral microbiota, we conducted a fostering experiment. As shown in Fig. 6F, adult offspring that lacked in utero exposure to maternal antibodies exhibited higher oral microbial loads, regardless of postnatal antibody transfer via breast milk. Next, we asked whether maternal antibodies also influence the adult oral mucosal immunity, specifically focusing on the gingiva as an important oral barrier. Analysis of the gingival leukocytes of adult mice revealed higher frequencies and numbers of CD4$^+$ and CD8$^+$ T cells in mIg^{neg} mice compared to mIg$^+$ mice (Fig. 6G, H and Supplementary Fig. 5). These results suggest that lacking maternal antibodies transferred in utero during early life disrupts the establishment of oral mucosal homeostasis in adulthood

Breast milk- and in utero-derived antibodies play distinct roles in maintaining oral epithelial integrity and regulating periodontal immunity

The altered homeostasis observed in the oral mucosa encourages us to ask whether the barrier function of the gingiva was also affected. For this, we profiled global gene expression in the gingiva of adult mIg^{neg} and mIg$^+$ mice. Hierarchical clustering identifies differential gene expression between the two groups of mice (Fig. 7A). GSEA revealed an elevation of immunological-associated pathways in mIg^{neg} mice such as inflammatory response, allograft rejection, UV response, IL-2/STAT5 signaling, and complement (Fig. 7B). In addition, pathways associated with tissue homeostasis and remodeling were upregulated in this group and include epithelial to mesenchymal transition, Kras singling, mitotic spindle, apical junction, hedgehog signaling, coagulation, and angiogenesis[22]. The GSEA also identified the down-regulation of various pathways related to tissue metabolism, such as oxidative phosphorylation, fatty acid metabolism, glycolysis, hypoxia, adipogenesis, myogenesis, and reactive oxygen species[25]. Other reduced pathways were associated with cell proliferation, such as MYC target genes, G2M checkpoint, DNA repair, E2F targets, and the p53 pathway.

Since several of the above-dysregulated pathways imply an alteration in the function of the gingival epithelium, we subsequently examined the gingival epithelium. Initially, epithelial permeability was assessed by administering FITC solution onto the oral epithelium of anesthetized mice and then quantifying FITC staining intensity within the gingiva. As depicted in Fig. 7C, higher fluorescence intensity was observed in gingival tissues isolated from mIg$^+$ mice compared to mIg^{neg} mice, indicating greater epithelial sealing in the latter. Corresponding with this finding, the expression of the tight junction protein ZO-1 was elevated in the epithelium of mIg^{neg} mice (Fig. 7D). qPCR analysis further revealed an upregulation of *Cldn1* and *Cldn4*, other types of tight junction molecules, in mIg^{neg} offspring, supporting their enhanced epithelial sealing (Fig. 7E). Agreeing with the upregulation of tissue remodeling pathways noted earlier, the gingival epithelial cells of adult mIg^{neg} mice exhibited increased BrdU incorporation upon treatment, suggesting a faster proliferation rate compared to mIg$^+$ mice (Fig. 7F). To assess the respective contributions of in utero versus breastfeeding-derived antibodies to epithelial development, a fostering experiment was performed. As shown in Fig. 7G, H, mice that received maternal antibodies via breastfeeding exhibited increased FITC penetration, reduced expression of tight junction genes, and downregulation of the proliferation-associated gene *Ki67*, suggesting a postnatal role in regulating oral epithelial maturation. Finally, perinatal antibiotic treatment, which reduced early-life microbial load, eliminated the differences in epithelial gene expression between mIg$^+$ and mIg$^-$ offspring (Supplementary Fig. 6), indicating that epithelial maturation depends on the ability of breast milk antibodies to limit microbial exposure during early life

https://doi.org/10.1038/s41467-026-71704-5

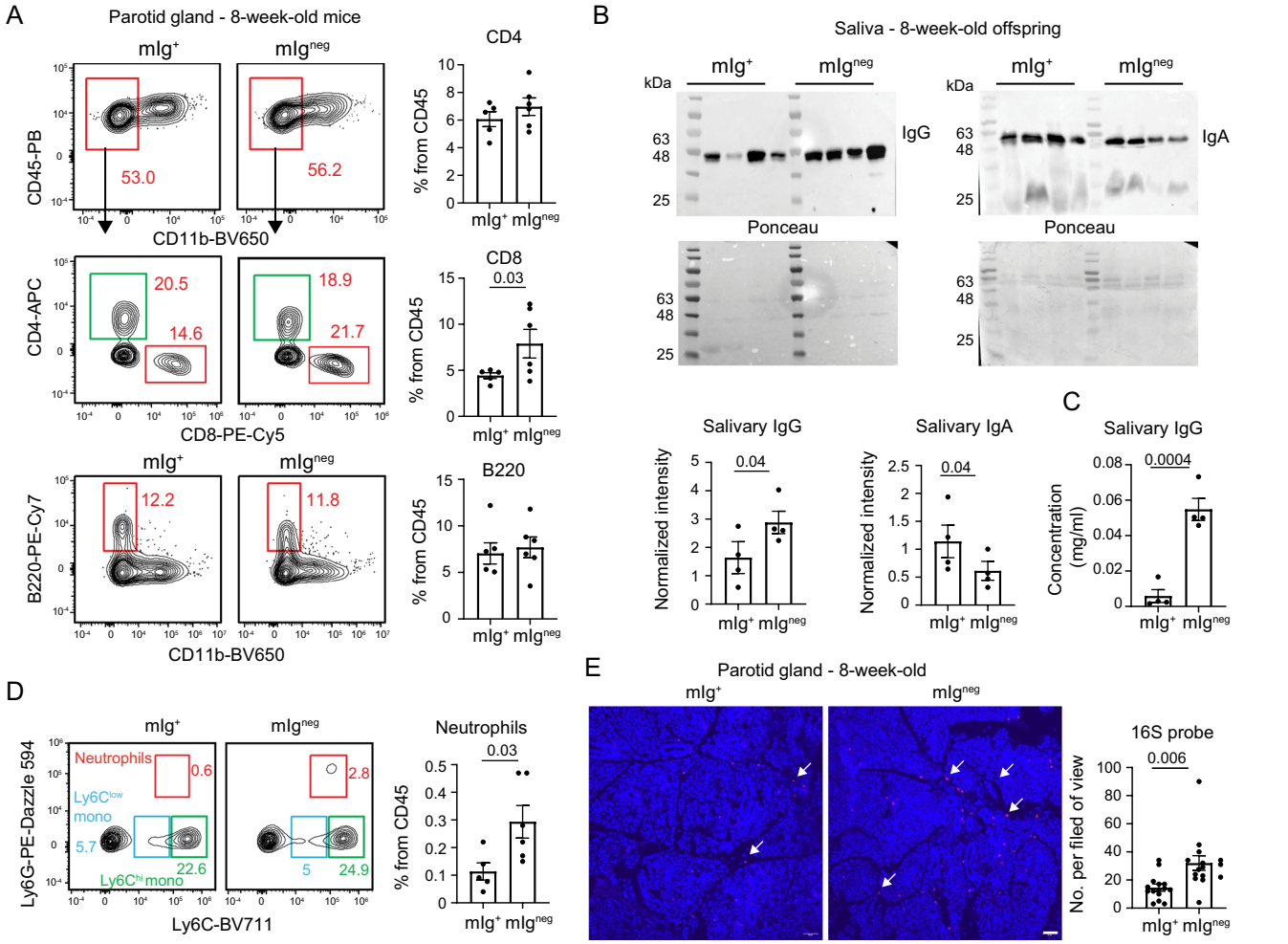

Fig. 5 | Maternal antibodies modify salivary immunity in adulthood. **A** Representative flow cytometry plots and graphs present the mean frequencies ± SEM (mIg$^+$ $n = 5$, mIg^{neg} $n = 6$) of CD4$^+$ T, CD8$^+$ T, and B cells in the parotid glands of 8-week-old mIg$^+$ and mIg^{neg} mice. Representative data of two independent experiments. **B** Western blot detection of IgG and IgA in the saliva of 8-week-old mIg$^+$ and mIg^{neg} mice. The graphs present the IgG and IgA levels ± SEM after normalization to total salivary proteins using Ponceau staining ($n = 4$). Representative data of three independent experiments. **C** Graph shows the mean IgG concentration ± SEM ($n = 4$) in the parotid gland of 8-week-old mIg$^+$ and mIg^{neg} mice, as measured by ELISA. Representative data from two independent experiments. **D** Flow cytometry plots and a graph show the mean frequencies ± SEM (mIg$^+$ $n = 5$, mIg^{neg} $n = 6$) of neutrophils in the parotid glands of 8-week-old mIg$^+$ and mIg^{neg} mice. Representative data of two independent experiments. **E** Visualization of bacterial 16S rRNA by a fluorescence probe (red) and DAPI (blue) in the parotid gland cross-sections of 8-week-old mIg$^+$ and mIg^{neg} mice. The arrows signify representatives labeled 16S rRNA. The graph shows the mean numbers ± SEM of 16S rRNA per field of view ($n = 15$ sections collected from 5 mice). Representative images of two independent experiments. Scale bar, 25 μm. Statistical analysis: *p*-value from a two-tailed, unpaired t-test using GraphPad Prism.

Next, we assessed natural bone loss around the teeth (the alveolar bone) in each group, as this type of bone is sensitive to changes in gingival health. While no significant differences were found in levels of natural bone loss (as indicated by the values of bone volume and the exposed root area), the alveolar bone of mIg^{neg} mice exhibited alterations in trabecular numbers and thickness (Fig. 7I). Accordingly, increased numbers of TRAP-positive cells, representing bone-resorbing osteoclasts, were observed in the maxilla of mIg^{neg} mice (Fig. 7J). To determine whether the altered oral mucosal homeostasis in mIg^{neg} mice increases their susceptibility to periodontal disease, we utilized the ligature-induced periodontitis (LIP) model, a well-established approach that triggers local inflammation and microbial dysbiosis leading to alveolar bone loss. As demonstrated in Fig. 7K, the mIg^{neg} mice exhibited elevated bone loss, the hallmark of periodontitis. The elevated bone loss was associated with higher frequencies of neutrophils and CD8$^+$ T cells (Fig. 7L and Supplementary Fig. 7), indicative of heightened periodontal immune responses. To dissect the respective contributions of in utero- versus breastfeeding-derived antibodies to gingival immunity, we performed LIP in fostered mice. As shown in Fig. 7M, mice lacking in utero maternal antibodies exhibited elevated bone loss, underscoring their pivotal role in gingival immune regulation. These results collectively suggest that maternal antibodies exert distinct effects on the adult gingival barrier. Antibodies transferred postnatally via breast milk regulate epithelial maturation, whereas those acquired in utero program gingival immunity and shape adult inflammatory responses and susceptibility to periodontitis. Figure 8 provides a schematic summary of the respective contributions of breast milk- and placentally-derived antibodies to offspring oral immunity.

Discussion

This study highlights the contribution of maternal antibodies to the postnatal establishment of salivary and oral homeostasis in offspring. While maternal IgG is supplied to the salivary and oral mucosa both prenatally and postnatally, our findings indicate that in utero-derived IgG exerts a more profound and lasting influence on salivary and oral mucosal immunity. In contrast, breast milk-derived IgG, and possibly IgA, primarily contribute to the postnatal maturation of the oral

https://doi.org/10.1038/s41467-026-71704-5

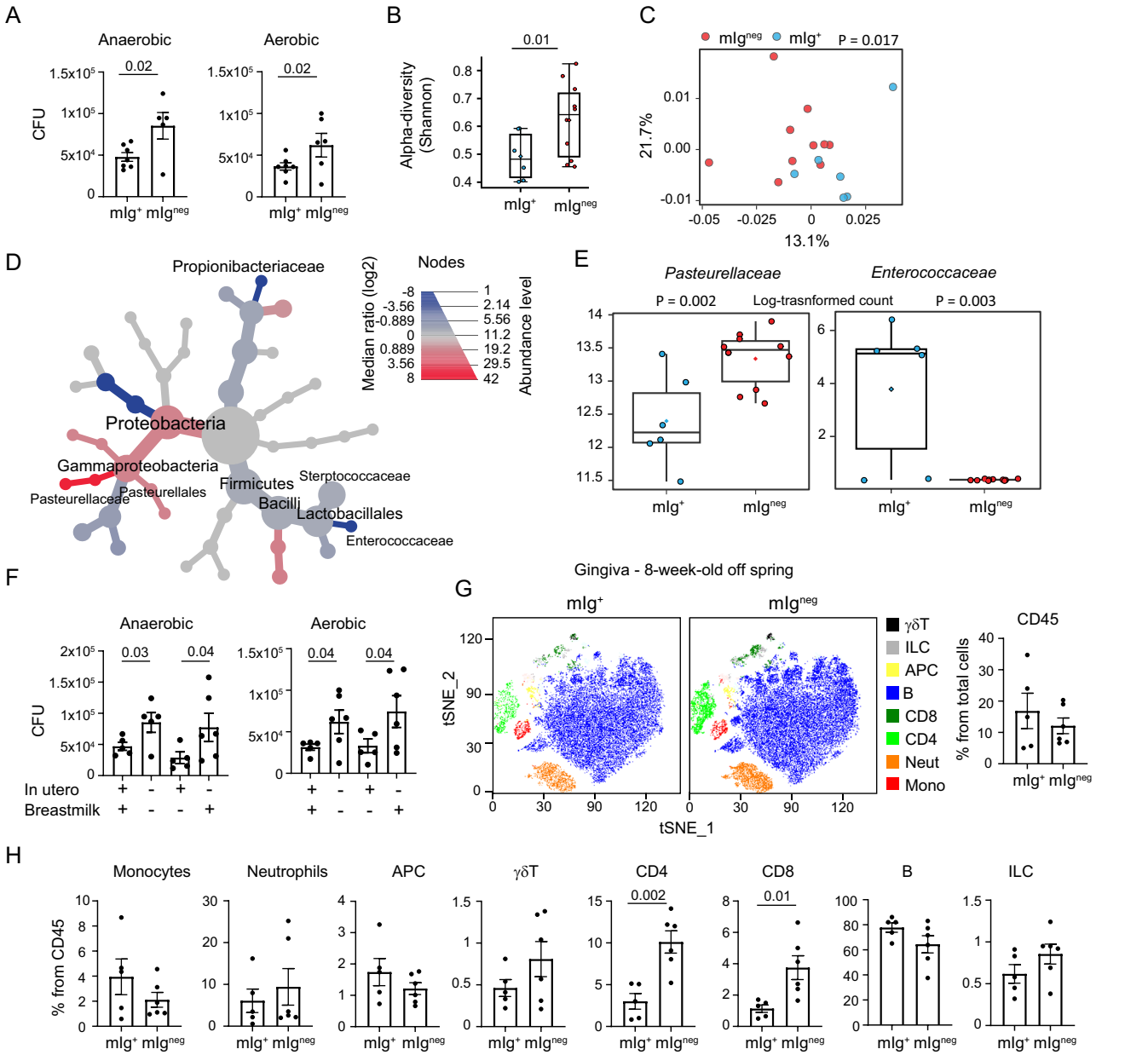

Fig. 6 | The absence of in utero-derived maternal antibodies disrupts the development of oral microbial and immunological homeostasis in adult life. **A** Quantification of cultivated aerobic and anaerobic bacteria collected from the oral cavity of 8-week-old mIg$^+$ and mIg^{neg} mice. The graph presents the mean c.f.u. ± SEM (mIg$^+$ $n = 7$, mIg^{neg} $n = 5$ and 6). Representative of two independent experiments. **B** Alpha diversity plot representing taxa richness in samples of both groups of mice. (mIg$^+$ $n = 6$, mIg^{neg} $n = 10$). Data represented as a standard boxplot, the median denoted as a central horizontal line in the box, and the whiskers covering the data within ± 1.5 IQR. Welch's two-sample t-test (MicrobiomeAnalyst) (**C**) PCA of weighted UniFrac distances based on 16S rRNA of mIg$^+$ and mIg^{neg} mice. **D** Heat tree showing microbiota differences between mIg$^+$ and mIg^{neg}. Significantly altered taxa are displayed by name at the corresponding node. Named nodes highlight significantly altered taxa. Red branches: increased in mIg^{neg}; blue branches: decreased. **E** Log-transformed counts of two bacterial families measured from mIg$^+$ and mIg^{neg}. (mIg$^+$ $n = 6$, mIg^{neg} $n = 10$). Data represented as a standard boxplot, the median denoted as a central horizontal line in the box, and the whiskers covering the data within ± 1.5 IQR. LEfSe analysis at the family level (FDR-adjusted $P < 0.1$, log LDA ≥ 2.0; MicrobiomeAnalyst). **F** Quantification of the CFU ± SEM (Anaerobic, $n = 5$ except for the -/+ group ($n = 6$); Aerobic, $n = 6$ except for +/+ and +/- groups ($n = 5$)) of aerobic and anaerobic oral microbiota in 8-week-old mice cross-fostered with $J_HT^{-/-}$ or $J_HT^{+/+}$ dams after birth. Representative data from two independent experiments. **G** t-SNE flow cytometry plots display the main subsets of leukocytes present in the gingiva of 8-week-old mIg$^+$ and mIg^{neg} mice. The graph shows the frequencies of CD45$^+$ lymphocytes ± SEM from the total cells (mIg$^+$ $n = 5$, mIg^{neg} $n = 6$). Representative data from two independent experiments. **H** Graphs show the mean frequencies ± SEM (mIg$^+$ $n = 5$, mIg^{neg} $n = 6$)of the various leukocytes in the gingival tissues of adult mIg$^+$ and mIg^{neg} mice. Representative data from two independent experiments. Statistical analysis: two-tailed unpaired t-test and one-way ANOVA.

epithelium, consistent with previous reports[29]. Maternal IgG binds a substantial fraction of neonatal bacteria and helps regulate immune responses, promoting host-microbiota mutualism during a critical postnatal period[14,16,30]. The distinct impacts of prenatal versus breast milk-derived antibodies likely reflect differences in timing and delivery. Prenatal IgG enters the circulation before microbial colonization begins, reaching the oral mucosa and interacting with immature immune cells and epithelial barriers. This early systemic delivery programs local immune tone and tolerance, shaping neonatal acceptance of oral microbiota. By contrast, breast milk IgG is introduced after birth, acting primarily through localized exposure to oral and gut microbiota, with its effects more vulnerable to disruptions such as

https://doi.org/10.1038/s41467-026-71704-5

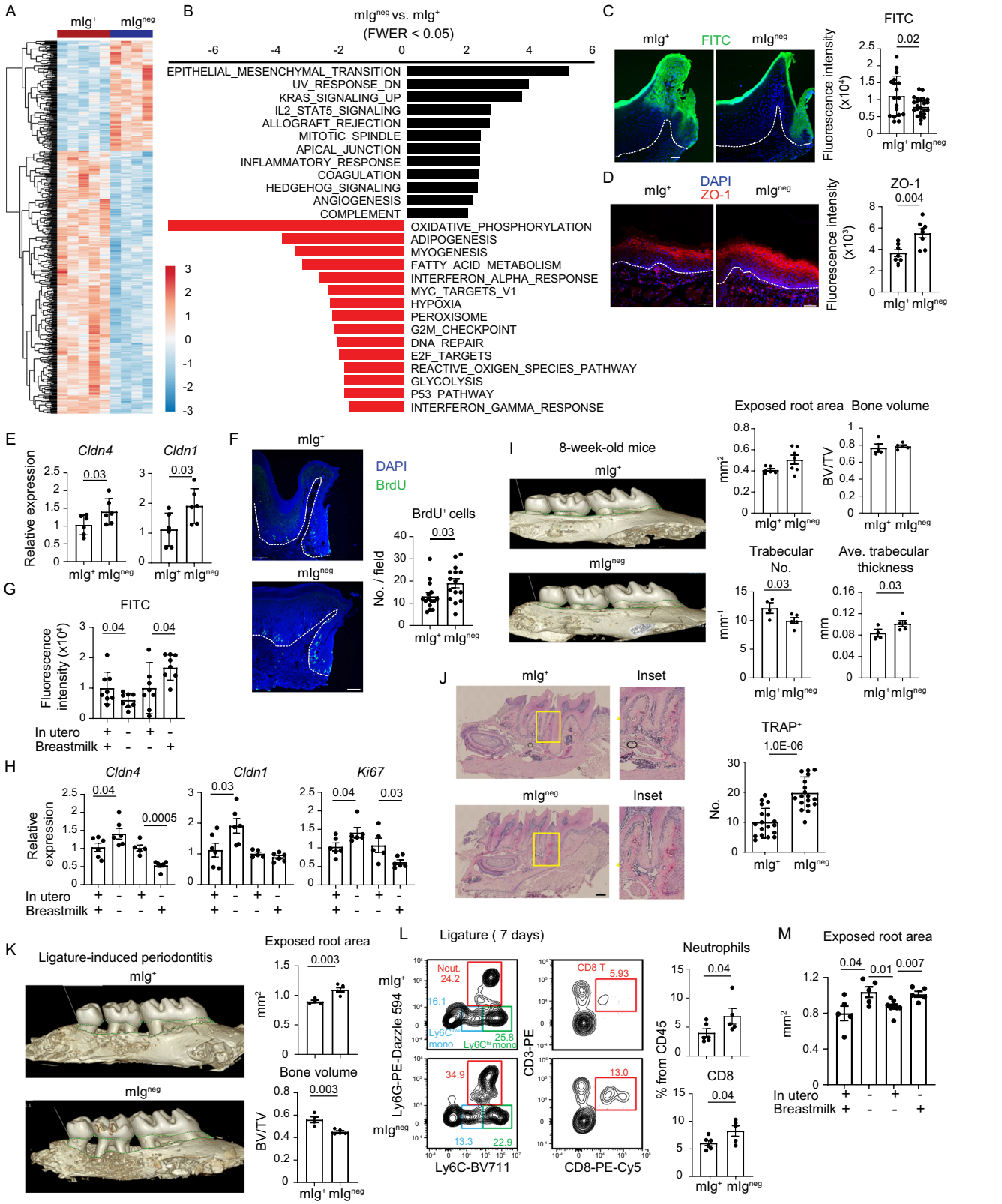

antibiotic treatment[30]. Consistent with this, we demonstrate that perinatal antibiotics impaired the impact of breast milk-derived antibodies but not those acquired prenatally.

The active transfer of dual-source IgG to the salivary glands appears to be a fundamental early-life mechanism guiding the development of the oral-salivary mucosal system. In contrast, breast milk-derived IgA antibodies are either absent or present only at very low levels in the salivary gland and saliva, respectively, thereby limiting their contribution to this process. Although nursing exposes the oral mucosa to elevated levels of IgA and IgG, this exposure is likely brief and insufficient to shape postnatal oral immunity. In line with this observation, we did not detect an effect of breast milk IgG on oral-salivary immunity, despite recent evidence that these antibodies can instruct the neonatal immune system toward gut antigens[30]. The

Fig. 7 | Breast milk- and in utero-derived maternal antibodies distinctly regulate adult gingival epithelial integrity and immune responses. A Hierarchical clustering of the genes differentially expressed in the gingiva of 8-week-old mIg$^+$ and mIg^{neg} mice ($n = 4–5$). **B** Significantly upregulated and downregulated gene pathways identified by GSEA among 8-week-old mIg$^+$ and mIg^{neg} mice gingival cells (FWER < 0.05). Representative of two experiments. (**C**) Gingiva from adult mIg$^+$ and mIg^{neg} mice showing FITC localization after topical application. Quantification of fluorescence intensity as mean ± SEM (mIg$^+$ $n = 18$ sections/6 mice; mIg^{neg} $n = 24$ sections/8 mice). Scale bar, 50µm. Representative of four experiments. **D** Immunofluorescence staining for ZO-1 with DAPI in the gingiva of 8-week-old mice. Graph shows MFI ± SEM ($n = 8$ sections/4 mice). Scale bar, 50 µm. Representative of two experiments. **E** Relative expression of indicated genes measured by qPCR and normalized to mIg$^+$ mice (mean ± SEM, $n = 6$). Representative of two experiments. **F** BrdU incorporation assay performed in 8-week-old mice. Images show BrdU$^+$ cells in the gingival epithelium 16 h post-injection. Quantification shows mean BrdU$^+$ cells±SEM ($n = 15$ sections from 5 mice). The dotted line indicates the basal membrane. Scale bar, 50 µm. Representative of two experiments. **G** Fluorescence intensity in the gingiva following topical FITC application in cross-fostered mice. Mean ± SEM ($n = 8$ sections from 4 mice). Representative of two experiments. (**H**) Relative gene expression in cross-fostered mIg$^+$ and mIg^{neg} mice measured by qPCR (mean ± SEM, n = 6; n = 5 for +/−). Representative of two experiments. **I** µCT analysis of adult maxillae showing exposed root area, alveolar bone volume, and trabecular parameters (exposed root area $n = 7$; mIg$^+$ $n = 4$, mIg^{neg} $n = 5$). **J** TRAP staining of gingival sections from adult mice. Graph shows mean TRAP$^+$ cells±SEM ($n = 18$ sections from 6 mice). Yellow arrows indicate TRAP$^+$ cells. Scale bar, 50µm. **K** LIP assessed 9 days post-placement. Bone loss measured as exposed root area and bone volume (mean ± SEM, $n = 5$). Representative of two experiments. **L** Flow cytometry analysis 7 days post-ligature showing frequencies ±SEM of neutrophils and CD8$^+$ T cells (mIg$^+$ $n = 6$, mIg^{neg} $n = 5$). Representative of two experiments. **M** Ligature-induced bone loss in cross-fostered mice (mean ± SEM; $n = 5$, $n = 8$ for +/−). Representative of two experiments. Statistical analysis: *p*-value from a two-tailed, unpaired t-test and an ordinary one-way ANOVA test using GraphPad Prism.

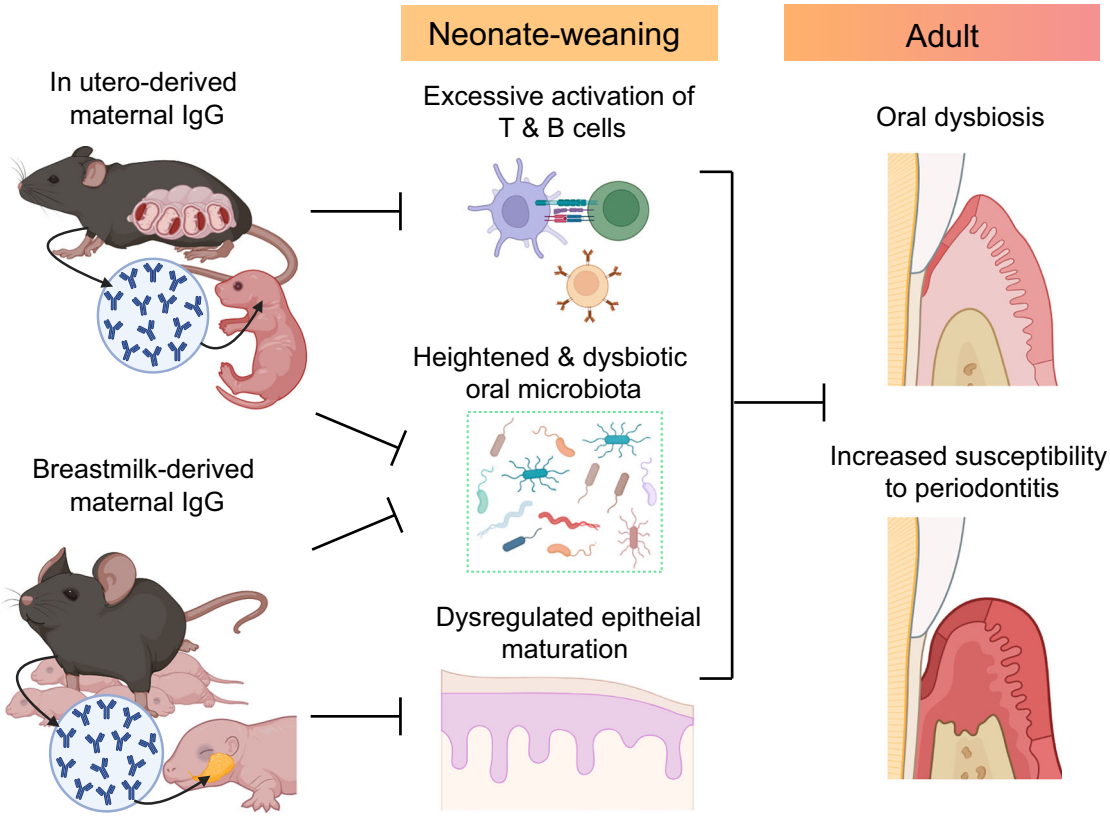

Fig. 8 | Schematic illustrating the distinct roles of in utero- and breast milk-derived antibodies in shaping oral mucosal immunity. Maternal IgG antibodies transferred to the offspring in utero and during breastfeeding are actively transported from the neonatal circulation to the salivary glands and subsequently secreted into the saliva. In utero-derived IgG has a major impact on postnatal development of the salivary glands and gingival immunity, restraining T- and B-cell immune responses. In contrast, breast milk-derived IgG regulates the timing of oral epithelial maturation, preventing premature epithelial differentiation and excessive barrier sealing after birth. Antibodies from both sources are capable of recognizing and binding the maternal oral microbiota, contributing to reducing the oral microbial load in neonates. Together, these coordinated actions shape oral mucosal homeostasis by modulating adult microbial load and composition, epithelial function, and baseline gingival immune activity, ultimately influencing susceptibility to periodontitis through exaggerated inflammatory responses to periodontal challenge that drive tissue destruction. Created in BioRender. Hovav, A. (2026) https://BioRender.com/0xcholr.

observed transfer of breast milk IgG to the salivary glands supports the notion that a sustained and higher antibody presence is required to influence the oral mucosa via the salivary system. Nevertheless, breast milk IgG and IgA may still bind microorganisms in the oral cavity, which at this stage is exposed to a heavy microbial load[1], enabling the translocation of opsonized microbes to the developing gut. Since the oral mucosa is the primary entry point for intestinal microbes, such opsonization by both prenatal and postnatal maternal antibodies may represent an additional mechanism through which maternal antibodies shape intestinal immunity.

Our results demonstrate that maternal IgG antibodies effectively recognize the oral microbiota of their maternal origin, consistent with previous gut studies showing comparable specificity and implicating FcRn-transferred maternal IgG in the regulation of neonatal immunity[16,20,30]. The FcRn receptor also mediates the transfer of maternal IgG from the circulation to breast milk and saliva[10,31],

suggesting a shared postnatal delivery pathway. In our study, maternal IgG reduced the neonatal oral microbial burden, a notable finding given that IgG is classically associated with systemic immunity via opsonization and phagocyte-mediated clearance[32]. This indicates an unconventional role for salivary maternal IgG in preventing bacterial attachment to the neonatal oral epithelium, paralleling effects described in the gut[16]. Furthermore, opsonization of oral microorganisms by maternal IgG may promote their phagocytosis by neutrophils present in saliva[33] and in the permeable neonatal oral epithelium, where neutrophil recruitment is high during early life[1].

Maternal IgG antibodies transferred prenatally and seeding neonatal salivary glands and saliva could engage Fcγ receptors on DCs, directing their recruitment and activation at oral mucosal surfaces, as evidenced in analogous immune compartments[34,35]. This mechanism likely accounts for the heightened DC migration to salivary glands observed in the absence of maternal IgG, accompanied by reduced Treg frequencies and persistent hyperactivation of T- and B-cells. In alignment with this, microbial exposure in GF mice promotes oral DC migration to salivary glands, where they activate T cells, emphasizing the microbiota-dependent role of salivary DCs in local immunity[10]. Transcriptional profiling reveals a bias toward IL-2-STAT5 signaling, allograft rejection, and inflammatory pathways in neonates lacking maternal IgG, alongside attenuated IFN-α responses, which fosters effector bias and destabilizes mucosal tolerance. Such activity could alter immunity in neonatal salivary glands, which at this developmental stage are enriched in $CD11b^{+}CD301a^{+}$ DCs that are known to promote Treg responses to commensal microbes[19]. Maternal IgG also likely modulates salivary immunity through multiple overlapping mechanisms, including generalized neonatal immune suppression[13], immune complex formation with microbiota engaging inhibitory FcγRIIB to suppress B-cell activation[36], and efficient IgG2b binding to oral microbiota via Fcγ receptors[37]. In this regard, the present study found that maternal IgG2b is the most abundant isotype transferred to the saliva of neonates. Notably, this regulatory effect endures despite perinatal antibiotic treatment, indicating intrinsic dampening by prenatal antibodies, though microbial signals remain crucial for adaptive priming, with additional contributions from antigen neutralization, Fc-dependent phagocytosis, and epitope masking to limit B-cell recognition[38,39].

Maternal IgG absence reprogrammed adult gingival transcriptomes toward epithelial-mesenchymal transition, proliferative spindling, and inflammatory/coagulation cascades, while suppressing OXPHOS and interferon responses, indicative of immature bioenergetics and lost homeostatic surveillance. This hyper-remodeling state aligns with elevated gingival effectors and fewer regulatory T cells, likely reflecting the unopsonized antigen's reliance on activating FcγR pathways over inhibitory FcRn-IgG complex handling and reduced FcγRIIB-mediated suppression on myeloid cells and B cells, promoting microbiota-driven barrier adaptation at the cost of chronic low-grade inflammation[14,30]. The oral microbiota also influences neonatal epithelial barrier function by regulating tight junction protein expression[1]. Thus, the elevated microbial burden in mice lacking maternal antibodies likely drives increased expression of these proteins, contributing to heightened epithelial sealing. The microbiota also promotes epithelial growth and proliferation, consistent with the elevated proliferative capacity observed in these mice. Supporting this, claudins and ZO-1, both upregulated in the absence of maternal antibodies, are known to regulate epithelial proliferation and survival[40]. Whether these traits are advantageous is uncertain: while they may prevent microbial invasion and protect against masticatory damage[41], excessive sealing can impair immune function by limiting DC access to microbial antigens, restricting controlled microbial sampling, and disrupting neutrophil transmigration, processes essential for periodontal health. Consistent with this, mIg^{neg} mice display elevated steady-state frequencies of $CD4^{+}$ and $CD8^{+}$ T cells in the gingiva, increased microbial load, and dysregulated epithelial signaling, all indicative of a dysbiotic environment. Such dysbiosis likely underlies the greater alveolar bone loss observed in these mice during experimental periodontitis, as heightened inflammatory responses drive excessive, immune-mediated destruction of alveolar bone.

Oral bacteria selectively targeted by maternal IgG, including *Pasteurellaceae*, *Burkholderiaceae* (*Betaproteobacteriales*), *Corynebacteriaceae*, and *Mycoplasmataceae*, exhibit invasive potential and are strongly associated with inflammatory oral disease[42]. *Pasteurellaceae*, particularly *Aggregatibacter actinomycetemcomitans*, are established drivers of aggressive periodontitis[43], while *Burkholderiaceae* species, though classically linked to systemic infections, have been implicated in severe oral-derived pathology[44]. *Corynebacteriaceae*, notably *Corynebacterium* spp., function as biofilm scaffolds and, under inflammatory conditions, act as opportunistic pathogens or markers of dysbiosis[45]. *Mycoplasmataceae* are enriched in the subgingival plaque of periodontitis patients and contribute to sustained inflammatory signaling[46,47]. In contrast, abundant taxa such as *Lactobacillus*, *Streptococcus*, *Staphylococcus*, and Bacteroides were not enriched by maternal IgG, suggesting that antibody binding reflects selective immune recognition rather than microbial abundance. These core commensals have limited capacity to disrupt mucosal integrity[48], and their exclusion from the IgG repertoire likely reflects active tolerance to preserve mucosal homeostasis. The adult oral microbiota was significantly altered in mice lacking maternal antibodies, with *Pasteurellaceae* (*γ-proteobacteria*) dominating compared to *Enterococcaceae* in controls. *Pasteurellaceae* expansion is favored by inflammation[42,49], and aligns with the elevated immune responses seen in these mice. This microbial shift likely primes the host for an exaggerated inflammatory response during ligature-induced periodontitis driven by the ability of *Pasteurella* to secrete toxins that activate the inflammasome and stimulate NF-κB signaling, leading to the excessive production of pro-inflammatory cytokines like IL-1β and IL-6[50]. This may explain the increased bone loss observed in experimental periodontitis[51]. Notably, ligatured gingiva from mice without maternal antibodies contained more $CD8^{+}$ T cells and neutrophils, consistent with recent findings that gingiva-resident $CD8^{+}$ T cells exacerbate periodontitis by promoting neutrophil enrichment[52].

Although maternally derived IgG is well established to cross the human placenta via FcRn and confer systemic immunity to the fetus, its presence and origin within the neonatal oral cavity remain incompletely defined. Multiple studies have detected IgG in the saliva of newborns and young infants, including a transient salivary IgG component preceding the maturation of secretory IgA responses, with salivary IgG levels correlating with maternal exposure or breastfeeding status[53–55]. These observations support the presence of maternally derived IgG in neonatal saliva, likely originating from the systemic circulation, though whether this occurs through active FcRn-mediated transcytosis or passive serum transudation remains unresolved. The demonstrated capacity of maternal antibodies to shape oral mucosal immunity provides a strong rationale for maternal immunization strategies aimed at enhancing offspring resistance to oral diseases such as periodontitis. Promising approaches include pregnancy-administered vaccines targeting dominant oral pathobionts such as *Porphyromonas gingivalis*, designed to preferentially elicit IgG2b/IgG1 responses, building on successful precedents for maternal immunization against enteric and respiratory pathogens[56,57], while acknowledging translational challenges related to species-specific FcRn kinetics, gestational timing of IgG transfer, and the uncertain relevance of active salivary IgG trafficking in humans.

In summary, this study expands our understanding of how the neonatal oral-saliva feedback loop regulates mucosal homeostasis after birth, while maternal IgG antibodies play a fundamental immunoregulatory role. It further reveals that the immunological influence

of maternal antibodies extends beyond neonatal life into adulthood, underscoring their significant impact on oral mucosal immunity.

Methods

Mice

C57BL/6 (B6) (The Jackson Laboratory, strain #: 3000664)and $J_HT^{-/-}$ (The Jackson Laboratory, strain #: 002438) mice were bred and maintained in the central animal facility at the Hebrew University Faculty of Medicine (Jerusalem, Israel). The mice were housed under specific pathogen–free (SPF) conditions in the institutional animal facility, maintained on a 12-hour light/12-hour dark cycle, at an ambient temperature of 22 ± 2 °C and relative humidity of 50–60%, with ad libitum access to food and water, and analyzed at various ages as described in the text. Control and experimental groups were housed separately, unless indicated otherwise in the text. All animal protocols were approved by the Hebrew University Institutional Animal Care and Use Committee (IACUC). The Germ-free (GF) B6 mice were maintained in sterile isolators at the Weizmann Institute of Science; the GF studies were approved by the IACUC of the Weizmann Institute of Science.

Antibodies

All antibodies, their catalogue numbers, final dilutions, and source are documented in Supplementary Table 1.

Isolation of oral leukocytes

The gingiva and the parotid gland tissues were excised into wells containing PBS-FBS 2%. Tissues were then minced and treated with a Collagenase type II (2 mg/mL; Worthington Biochemicals) and DNase I (1 mg/mL; Sigma) solution in PBS plus 2% FCS for 25 min at 37 °C in a shaker bath (for the list of reagents used in this study, see Supplementary Table 3)A total of 20 µL of 0.5 M EDTA per 2 mL sample was added to the digested tissues and incubated for an additional 10 min. The cells were washed, filtered with a 70-µM filter, stained with antibodies, run in an Aurora (Cytek) flow cytometer, and further analyzed, generating plots and t-SNE plots using FlowJo software (BD Biosciences).

T-cell stimulation assay

For intracellular cytokine staining, purified gingival cells were stimulated with phorbol myristate acetate (PMA) (1 mg/mL)/ionomycin (1 mg/mL) and Golgi Plug (2 mL/mL) for 6 hours at 37 °C. The cells were then stained with CD45, CD3, CD4, CD8, and αβTCR antibodies, permeabilized using BD Cytofix/Cytoperm™ kit (BD Biosciences), and then stained with IL-17A and IFN-γ antibodies. The samples were run in the Aurora (Cytek) flow cytometer and further analyzed using FlowJo software (BD Biosciences).

Immunofluorescence staining

For frozen section staining, the maxilla was fixed overnight at 4 °C in 4% paraformaldehyde/PBS solution and then decalcified for 2–3 weeks in EDTA 0.5 M/PBS. The tissue was cryopreserved in 30% sucrose (overnight at 4 °C), embedded in OCT, and cryo-sectioned into 10-µm-thick sections. The cross-sections were washed 3 times in PBS, blocked in blocking buffer (5% FCS, 0.1% Triton X-100 in PBS) for 1 hour at room temperature, and incubated with a primary antibody overnight at 4 °C. Following 3 washing steps in PBS, the samples were incubated with a secondary antibody diluted 1:200 in blocking buffer for 2 hours at room temperature, washed 3 times, stained with DAPI, and mounted. For paraffin sections, the maxilla was fixed overnight at 4 °C in 4% paraformaldehyde/PBS solution and then decalcified for 2–3 weeks in EDTA 0.5 M/PBS, which was changed every other day. The tissues were dehydrated using 70%, 80%, 90%, and 100% ethanol and then xylene to dissolve the alcohol. Next, the tissues were embedded in paraffin and micro-sectioned into 7 µm-thick sections. Slides were deparaffinized with xylene, and 100%, 95%, 80%, and 70% ethanol washed 3 times with PBS, blocked in blocking buffer (PBS, 10%FCS, 10% BSA, 2% Triton X-100) for 1.5 h at room temperature, and incubated with primary antibodies at 4 °C. Following 3 washing steps in PBS, the samples were incubated with secondary antibodies diluted 1:200 in blocking buffer for 1.5 hours at RT, washed 3 times, stained with DAPI, and mounted. As a negative staining control, the primary antibody was omitted and replaced with the blocking buffer. Signals were visualized, and digital images were obtained using a Nikon spinning disk confocal microscope.

Fluorescent in Situ Hybridization for 16S ribosomal RNA

For fluorescent in situ hybridization (FISH) analysis, the tissues were excised and fixed overnight at 4 °C in 4% paraformaldehyde/PBS solution. The tissues were dehydrated using 70%, 80%, 90%, and 100% ethanol and then xylene to dissolve the alcohol. Next, the tissues were embedded in paraffin and micro-sectioned into 7 µm-thick sections. Slides were deparaffinized with xylene, and 100%, 95%, 80%, and 70% ethanol and washed 3 times with PBS, dried, and stained with 1:100 with universal 16S probe in pre-warmed to 46 °C hybridization solution (20 mM Tris–HCl, pH 7.4, 0.9 M NaCl, 0.1% (w/v) SDS). The slides were then sealed with a cover slip and incubated in a humid chamber overnight at 46 °C. Following the 3 washing steps in PBS, the samples were stained with DAPI and mounted. As a negative staining control, a nonsense probe control was replaced with the 16S probe. Signals were visualized, and digital images were obtained using a Nikon spinning disk confocal microscope.

Hematoxylin and tartrate-resistant acid phosphatase staining

The maxilla was fixed overnight at 4 °C in 4% paraformaldehyde/PBS solution and then decalcified for 2–3 weeks in EDTA 0.5 M/PBS, which was changed twice a week. The tissues were dehydrated using 70%, 80%, 90%, and 100% ethanol and then xylene to dissolve the alcohol. Next, the tissues were embedded in paraffin and micro-sectioned into 7 µm-thick sections. Slides were deparaffinized with xylene, and 100%, 95%, 80%, and 70% ethanol and washed three times with PBS. TRAP (Sigma-Aldrich, Rehovot, Israel) staining with hematoxylin counterstain according to the manufacturer's instructions enabled quantification of the osteoclasts (TRAP-positive multinucleated cells at the alveolar bone surface). Images of TRAP-stained cross-sections were captured with a Nikon TL microscope.

BrdU incorporation assays

8-week-old mice were injected once intraperitoneally with BrdU, 10 µL/gram of body weight (Sigma). Gingival tissues were collected after 16 hours and then embedded in OCT and cryo-sectioned into 10 µm-thick sections. The cross sections were washed 3 times in PBS, incubated for 1 hour with 1 N HCl at 37 °C, and blocked in blocking buffer (20% FCS, 0.1% Triton X-100, 0.02% NaN3, 0.05% Tween-20 in PBS) for 1 hour at RT, and incubated with anti-BrdU antibody (Abcam) overnight at 4 °C. Following 3 washing steps in PBS, the samples were incubated with a secondary donkey anti-Sheep IgG H&L (Alexa Fluor 488) (Abcam), diluted 1:200 in dilution buffer (2% FCS, 0.1% Triton X-100, 0.02% NaN3, 0.05% Tween-20 in PBS) for 2 hours at RT, washed 3 times, stained with DAPI, and mounted. Signals were visualized, and digital images were obtained using a Nikon spinning disk confocal microscope.

Micro-computed tomography analysis

The hemi-maxillae were secured in an acrylic mold using orthodontic wax for stability during act scans, which were conducted at 8 µm resolution using a µCT instrument Skyscan1272 (Bruker microCT, Kontich, Belgium). Air served as the scan medium to optimize the contrast between the sample and the background. 3D reconstruction and analysis of the µCT images were executed using Dragonfly software [Version 2022.2 for Windows; Object Research Systems (ORS)

Inc., Montreal, Canada] with TIFF files. Bone volume evaluation was conducted between the mesiobuccal and distal roots of M2, utilizing the Bone Analysis Wizard. A 0.2 mm radius sphere was chosen to measure properties in 3D. Otsu's threshold method was employed to segment bone from non-bone; in our case, teeth were manually erased from the analysis since the software cannot distinguish between bone and teeth. The Bone Analysis module in Dragonfly was utilized to segment cortical and trabecular bone. Another adjustment made in the wizard was to disregard cortical bone, as it is very thin in mouse maxillae and cannot be distinguished by the software. After delineating all bone structures, bone morphometric measurements were computed, following the guidelines described by Bouxsein et al.[58], Using the Bone Analysis module, trabecular bone volume fraction (BV/TV), trabecular thickness (Tb.Th, μm), and trabecular number (Tb.N, 1/mm) were determined for trabecular bone. In the second method, DICOM files were extracted from the scanner and analyzed in the OnDemand3D Application. The area between the cementoenamel junction and the alveolar bone level was marked and measured on the buccal and palatal sides.

RNA extraction and qPCR

For RNA isolation, the excised gingiva was homogenized in 500 μl TRI reagent (Sigma) using an electric homogenizer (IKA labortechnik), and RNA was extracted according to the manufacturer's instructions. cDNA synthesis was performed using the qScript cDNA Synthesis Kit (Quanta-BioSciences). qPCR reactions (20 μL volume) were performed using Power SYBR Green PCR Master Mix (Quanta-BioSciences) and specific primers to the examined gene. The following reaction conditions were used: 10 min at 95 °C, 40 cycles of 15 s at 95 °C, and 60 s at 60 °C. The samples were normalized to 18S as a control mRNA using the change in cycling threshold (ΔCT) method and calculated based on the 2-ΔΔCT formula. The sequences of all primers used in this study are provided in Supplementary Table 2.

RNA-Seq differential expression analysis

Raw reads were processed according to the QuantSeq User Guide recommendations. Reads were trimmed at their 5′ end to remove the first 12 bases, then low-quality and technical bases were removed from the 3′ end using cutadapt (version 1.12)[59]. Finally, low-quality reads, with more than 30 percent of the bases with quality below 20, were filtered out using the FASTX package (version 0.0.14). Processed reads were aligned against the mouse genome using TopHat (v2.1.1)[60]. The genome version was GRCm38, with annotations from Ensembl release 89. Htseq-count (version 0.6.0)[61] was then used for quantification of raw counts per gene per sample, excluding short or otherwise unwanted gene types, such as rRNA or miRNA. Normalization and differential expression analysis were performed with the DESeq2 package (version 1.12.4)[62]. Genes with a sum of counts less than 10 over all samples were filtered out before normalization. Differential expression, comparing control (mIg^{+}) and treated (mIg^{neg}) groups, was calculated with default parameters, except that the independent filtering algorithm was used. The statistical significance threshold was taken as an adjusted *P*-value (padj) less than 0.1. Exact commands with the full parameters used can be found under GEO accession GSE274186.

Gene set enrichment analysis

The whole differential expression data were subjected to gene set enrichment analysis using GSEA[63]. GSEA uses all differential expression data (cut-off independent) to determine whether a priori–defined sets of genes show statistically significant, concordant differences between two biological states. GSEA was run against the hallmark gene set collection from the molecular signatures database (MSigDB, v6.2, July 2018).

Western blot analysis

Parotid gland or gingival tissues were isolated and homogenized in ice-cold lysis buffer (50 mM Tris pH 7.5, 150 mM NaCl, 1% Triton X-100, 0.5% NP-40, 0.1% SDS, 0.5 mM EDTA) supplemented with a protease inhibitor cocktail (Sigma). Following homogenization, tissue debris was removed by centrifugation (15,000 *g* for 10 min at 4 °C), and protein concentration was determined using a NanoDrop spectrophotometer. Samples were prepared by adding Tris-Glycine-SDS Sample Buffer followed by 2% β-mercaptoethanol (Sigma-Aldrich), and then heated at 90 °C for 10-15 min. Equal amounts of protein (50 μg) were loaded onto 7.5% acrylamide gels and resolved by SDS-PAGE. Proteins were transferred to Trans-Blot Turbo Mini nitrocellulose membranes (Bio-Rad) using the Trans-Blot Turbo Transfer System at 25 V, 1.3 A for 7 min. Membranes were blocked with PBS containing 0.05% Tween-20 (PBST) and 5% non-fat dried milk for 1 hour at room temperature, and incubated overnight at 4 °C on a shaker with HRP-conjugated goat primary antibody (1:5000 dilution in blocking buffer). The membrane was then washed 3 times in PBST before the blots were reacted with ECL substrate (Western blot detection kit, Advansta). Images were captured using a ChemiDocTM MP Image System (Bio-Rad). Bands were normalized to the band intensity of GAPDH.

ELISA and serum analysis

Blood was drawn from mice, and the sera were stored at −80 °C. Maternal microbiota was collected by swabs and enriched on blood agar overnight. Ninety-six-well plates (Nunc) were coated overnight at 4 °C with maternal microbiota in 0.1 M bicarbonate buffer (pH 9). The plates were washed twice with PBST and blocked with PBS 10% FCS (2 hours at room temperature). Subsequently, mouse serum samples diluted serially in PBS were added to the wells for 3 hr incubation at RT. This was followed by four washes in PBST and the addition of anti-mouse peroxidases-conjugated IgG1, IgG2a, and IgG2b, IgG3, IgA, and IgM antibodies (Southern Biotech). After incubation for 2 hours at RT, the plates were washed five times, and 100 μL/well of tetramethyl benzidine (TMB) solution (Southern Biotech) was added for 5 min, followed by the addition of 100 μL of TMB stop solution (Southern Biotech). Absorption was read at 450 nm using MULTISKAN SkyHigh (Thermo Scientific). For general characterization of antibody subtypes presented in the neonate's serum, we used the SBA Clonotyping System-HRP kit (Southern Biotech) according to the manufacturer's instructions. For quantifying IgG concentrations in the parotid glands, saliva, and serum, an IgG competitive inhibition ELISA kit (USCN Life Science Inc.) was used according to the manufacturer's protocol.

Microbiota analysis

The oral cavity of anesthetized B6 mice was swabbed for 30 seconds. The swabs were then processed for DNA isolation using the Zymo Quick-DNA Fungal\Bacterial DNA Extraction Kit according to the manufacturer's instructions. Library preparation, sequencing, and analysis were performed by Hay Laboratories (Israel) as follows: Libraries were prepared using a two-step PCR protocol. Primers 515F−806 R, which target the V4 region of the 16S SSU rRNA, were used for PCR amplification. 515 F (ACACTGACGACATGGTTCTACAGTGC CAGCMGCCGCGGT) and 806 R (TACGGTAGCAGAGACTTGGTCTG GACTACHVGGGTWTCT) (Earth Microbiome Project). The PCR reaction products were cleaned using AMPure beads and then subjected to a second PCR using the Fluidigm Access Array Primers for the addition of Illumina adaptor and index sequences. DNA was purified using Kapa Pure Beads at a ratio of 0.65X and quantified with Qubit using Denovix dsDNA high sensitivity assay. DNA size and integrity were quantified by Tapestation using Agilent DNA screen tape and reagents. The libraries were then sequenced on a dedicated MiSeq (Illumina) machine with 5-30% PhiX using MiSeq Reagent Kit v2 500PE. Demultiplexing was performed using bcl2fastq with default parameters, allowing for 0 mismatches. Data was then mapped to PhiX using bowtie2 to remove

PhiX control, and unmapped reads were quantified, collected, and examined using fastQC. Bioinformatics analysis was performed with QIIME 2. Briefly, demultiplexed fastq files were processed for adapter sequence removal using the Cutadapt trim-paired plugin, followed by denoising with DADA2 (via q2-dada2) to identify all observed amplicon sequence variants (ASVs). ASVs were aligned with Mafft (via q2-alignment) and used to construct a phylogeny with Fasttree2 (via q2-phylogeny). Taxonomy was assigned to ASVs using the q2-feature-classifier classify-sklearn naïve Bayes taxonomy classifier, which was pretrained against sequences extracted from Greengenes 13_8 99% OTUs sequences using primers set 515F-806R. Qiime2 output files were used as inputs to 'MicrobiomeAnalyst—comprehensive statistical, visual and meta-analysis of microbiome data' online tool (https://www.microbiomeanalyst.ca/MicrobiomeAnalyst/home.xhtml), after minor manual format editing.

To examine the absolute abundance of certain bacteria, DNA was prepared from oral swabs using the Zymo Quick-DNA Fungal\Bacterial DNA Extraction Kit according to the manufacturer's instructions, and then directly subjected to RT-PCR analysis using designated primers. qPCR reaction was performed using Power SYBR Green PCR Master Mix (Quanta-BioSciences Inc.). The following reaction conditions were used: 10 min at 95 °C, 40 cycles of 15 sec at 95 °C and 60 sec at 60 °C. The samples were normalized to the 18S as control mRNA by the change in cycling threshold (ΔCT) method, and calculated based on 2-ΔCT.

Permeability assay

20 mg of FITC (Sigma) was dissolved in 100 µl DMSO (Sigma) and then diluted 1:10 with acetone. The FITC solution was applied using a pipette on the buccal mucosa of anesthetized 8-week-old mice (40 µL per mouse). After 30 minutes, the mice were euthanasied with isoflurane in a desiccator, the oral cavity was washed with DDW, and the buccal tissues were collected, embedded in OCT, and cryosectioned into 10-µm-thick sections. Signals were visualized, and digital images were obtained using an Olympus BX51 fluorescence microscope. For toluidine blue experiments, 40 mg of toluidine blue was dissolved in 250 µL DMSO (Sigma) and then diluted 1:1 with acetone. The toluidine blue solution was applied using a pipette on the buccal mucosa of anesthetized 1-week-old mice (20 µL per mouse) or 8-week-old mice (50 µL per mouse). After 30 minutes, the mice were euthanasied, and the buccal tissues were collected, embedded in OCT, and cryosectioned into 10-µm-thick sections. Signals were visualized, and digital images were obtained using a Nikon spinning disk confocal microscope.

Epithelium permeability to IgG antibodies

One-week-old and eight-week-old mice were anesthetized, and 5 or 15 µL (adjusted based on body weight ratio) of Pacific Blue anti-mouse CD45.2 antibody (0.5 mg/mL) was carefully applied to the gingiva. After 30 minutes, the mice were euthanasied with isoflurane in a desiccator, and the oral epithelium was collected, processed to obtain a single-cell suspension, and analyzed using an Aurora flow cytometer (Cytek).

FITC application

20 mg of FITC (Sigma) was dissolved in 100 µL DMSO (Sigma), and the solution was diluted in acetone (1:1). Mice were anesthetized, and 40 µL of the solution was carefully applied to the gingiva. The parotid glands were excised 2 days after the application for flow cytometry analysis.

Fostering experiments

Pregnant $J_HT^{+/+}$ and $J_HT^{-/-}$ dams were timed-mated to deliver simultaneously, and within 24 hours of birth, the dams and offspring were exchanged to generate four groups: (1) mIg^+ pups nursed by $J_HT^{+/+}$ dams, (2) mIg^{neg} pups nursed by $J_HT^{-/-}$ dams, (3) mIg^+ pups nursed by $J_HT^{-/-}$ dams, and (4) mIg^{neg} pups nursed by $J_HT^{+/+}$ dams. Pups were fostered with litters of matching size and sex distribution to ensure equal nutritional access and maternal care. Cross-fostering was confirmed by daily monitoring of maternal behavior and pup survival. Tissues were collected at the indicated timepoints for downstream analysis.

Perinatal broad-spectrum antibiotic treatment

Pregnant dams were provided with a combination of amoxicillin (80 mg/L) and tylosin (40 mg/L) in their drinking water starting from embryonic day 15 until their offspring reached 4 weeks of age. The antibiotic-containing water was replaced every three days to maintain potency. Control dams received regular drinking water. All treatments were administered ad libitum.

IgG-Seq analysis

To assess the binding specificity of maternal antibodies to oral bacteria, we performed IgG-Seq using serum from 2-week-old mIg^+ and mIg^{neg} offspring. Due to the limited bacterial biomass obtained from direct oral swabbing, oral bacteria were isolated from swabs collected from the respective dams and cultured on blood agar under aerobic and anaerobic conditions to generate sufficient material (termed input microbiota) for downstream analysis. Bacterial colonies were harvested by centrifugation, washed in PBS, and resuspended to a standardized optical density (OD600). Aliquots of the cultured bacteria were incubated with heat-inactivated serum (1:100 dilution) from 2-week-old mIg^+ or mIg^{neg} offspring for 30 min at 4 °C. After washing to remove unbound antibodies, IgG-coated bacteria were labeled with PE-conjugated anti-mouse IgG antibody, followed by magnetic separation using an Anti-PE MicroBeads UltraPure system (Miltenyi Biotec). The labeled suspension was loaded onto a pre-equilibrated magnetic column and washed multiple times with PBS to remove unbound material. The IgG-bound ("positive") fraction was then eluted by removing the column from the magnetic field.

DNA was extracted using 270 µL of GT lysis buffer and 30 µL of proteinase K (both from the MagCore Genomic DNA Tissue Kit), combined with 200 µL of the sample in bead beating tubes (Type C, GeneAid). Bead beating was carried out for 2 min using a Biospec homogenizer. Samples were then incubated at 60 °C for 2 hours and subsequently processed on the MagCore extraction system (RBC Bioscience) using the MagCore Genomic DNA Tissue Kit cartridges and standard protocol.

For DNA amplificationan initial PCR was performed using 2 µL of DNA as template in a 25 µL reaction volume with PCRBio Hot Start Ready Mix and custom primers targeting the V4 region of the 16S rRNA gene (based on the Earth Microbiome Project). These primers included CS1/CS2 adapter sequences. Amplification was carried out for 25 cycles. Primer sequences: CS1_515F (V4_F): ACACTGACGACATGGTT CTACAGTGCCAGCMGCCGCGGT and CS2_806R (V4_R): TACGGTAGC AGAGACTTGGTCTGGACTACHVGGGTWTCT. 2 µL of the PCR product (containing CS1/CS2 adaptors) was used as template in a 10 µL reaction for 10 additional cycles using the Fluidigm Access Array Barcode Library protocol (2 µL barcode per reaction). Following amplification, DNA was purified using KAPA Pure Beads at a 0.65× ratio and quantified using Qubit with the DeNovix dsDNA High Sensitivity Assay. DNA fragment size and integrity were assessed using the Agilent TapeStation system with DNA ScreenTape and reagents.

Samples were then sequenced on a dedicated Illumina MiSeq instrument using the MiSeq Reagent Kit v2 (500-cycle, paired-end) with 30% PhiX spike-in. Demultiplexing was performed using *bcl2fastq* with default settings, allowing zero mismatches in the index reads. Reads were then aligned to the PhiX genome using *Bowtie2*, and unmapped reads were retained for downstream analysis. Read quality was assessed using *FastQC*.

For sequencing analysis, demultiplexed reads were imported into the CLC Genomics Workbench (Qiagen) and analyzed using the built-in

16S Microbiome pipeline. The workflow included quality filtering, adapter trimming, and OTU clustering under default parameters. Reads with a Phred quality score below 25 or length <150 bp were discarded, and a maximum of two ambiguous nucleotides per read was allowed. Only reads between 200 and 500bp were retained. Chimeric sequences and singletons were identified and removed. Remaining high-quality sequences were clustered into operational taxonomic units (OTUs) by alignment to the SILVA database at 97% sequence similarity.

Bacterial adhesion assay

Oral swabs were obtained from dams via swabbing and cultured on blood agar plates under aerobic and anaerobic conditions to generate sufficient bacterial biomass. Colonies were harvested, resuspended in sterile PBS, and adjusted to a standardized optical density. Bacterial suspensions were incubated with heat-inactivated serum (1:10 dilution) from 2-week-old offspring for 1 hour at 4 °C with gentle rotation to allow antibody binding. For the adhesion assay, immortalized oral epithelial cells (4NQO-L) were seeded in 24-well plates and cultured overnight in DMEM (Sigma-Aldrich, Rehovot, Israel) supplemented with 10% fetal calf serum, 2 mM L-glutamine, penicillin (100 units/mL), and streptomycin (100 μg/mL; Biological Industries, Beit Haemek, Israel). The cells were cultured at 37 °C and 5% CO2 until they reached confluence. Before infection, cells were washed with pre-warmed DMEM 10% FCS 1% L-glutamine 1% medium, washed, and then incubated with the serum-opsonized bacteria at a multiplicity of infection of 1:100 for 1 hour at 37 °C in 5% CO_2. Following incubation, wells were washed extensively with PBS to remove non-adherent bacteria. Cells were then lysed, and serial dilutions of the lysates were plated on blood agar to quantify adherent bacteria by CFU enumeration.

Phagocytosis assays

Oral bacteria were collected from dams via swabbing and cultured on blood agar plates under aerobic and anaerobic conditions. Bacterial colonies were harvested, washed in sterile PBS, resuspended, and incubated with heat-inactivated serum (1:10 dilution) from 2-week-old offspring for 1 hour at 4 °C with gentle rotation to allow opsonization. RAW264.7 cells were seeded in 24-well plates and cultured overnight in DMEM (Sigma-Aldrich, Rehovot, Israel) supplemented with 10% fetal calf serum, 2 mM L-glutamine, penicillin (100 units/mL), and streptomycin (100 μg/mL; Biological Industries, Beit Haemek, Israel). The cells were cultured at 37 °C and 5% CO_2. Cells were then exposed to opsonized bacteria at a multiplicity of infection (MOI) of [1:100] for 1 hour at 37 °C and 5% CO_2. After incubation, cells were washed thoroughly with sterile PBS to remove extracellular bacteria. Extracellular bacteria were killed by treatment with 6 mg/mL Metronidazole (Sigma-Aldrich) and 0.3 mg/mL Gentamycin (Biological Industries) for 1 hour. The medium was then replaced with complete DMEM, cells were incubated for 1 hour, and then lysed in sterile distilled water for 20 minutes. Lysates were plated on blood agar to quantify internalized bacteria by CFU enumeration. In a separate experiment, oral bacteria collected from dams were labeled with 10 μM CFSE (carboxyfluorescein succinimidyl ester; Invitrogen) in PBS for 1 hour at room temperature, with shaking in the dark. Excess dye was removed by three washes in 15 mL PBS. The labeled bacteria were then incubated with heat-inactivated serum from 2-week-old offspring (1:20 dilution) for 1 hour at 4 °C with gentle rotation to allow for antibody opsonization. Freshly isolated neutrophils (0.5 million), obtained from the femurs of adult WT mice using a Histopaque density gradient, were then added to the opsonized CFSE-labeled bacteria at a multiplicity of infection (MOI) of 10:1 and incubated at 37 °C for 30 min. After incubation, cells were thoroughly washed with cold PBS and stained with anti-Ly6G antibody to identify neutrophils. Phagocytosis was assessed by flow cytometry.

Experimental periodontitis

Mice were anesthetized, and silk ligatures (5/0, SMI, Belgium) were tied around both second maxillary molars as previously described (Abe and Hajishengallis 2013). Seven to nine days after ligature placement, the mice were euthanasied with isoflurane in a desiccator and analyzed.

Quantification of saliva flow

Mice were held at a 45° angle (head down), and the oral cavity was filled with a cone-shaped sponge for 15 minutes. The sponge was then inserted into a 0.5 mL tube with a hole in the bottom that was placed in a 2 mL tube and centrifuged for 3 min at 5000 *g*.

Quantification and statistical analysis

Data are expressed as means ± SEM. Statistical tests were performed using a two-sided, unpaired t-test comparing two groups, and a one-way ANOVA comparing more than two groups. A p-value of <0.05 was considered significant. Detailed information on the number (n) of biological samples and animals used is mentioned in the figure legends. $^{*}P < 0.05$ $^{**}P < 0.01$, and $^{***}P < 0.00.1$.

Data availability

The RNA-seq data generated in this study have been deposited in the NCBI Gene Expression Omnibus GEO database under accession codes GSE274186 and GSE316211. All data are included in the Supplementary Information or available from the authors, as are unique reagents used in this Article. The raw numbers for charts and graphs are available in the Source Data file whenever possible. Source data are provided with this paper.

References

1. Koren, N. et al. Maturation of the neonatal oral mucosa involves unique epithelium-microbiota interactions. *Cell Host Microbe* **29**, 197–209.e195 (2021).
2. Nassar, M. et al. GAS6 is a key homeostatic immunological regulator of host-commensal interactions in the oral mucosa. *Proc. Natl. Acad. Sci. USA* **114**, E337–E346 (2017).
3. Capucha, T. et al. Sequential BMP7/TGF-beta1 signaling and microbiota instruct mucosal Langerhans cell differentiation. *J. Exp. Med.* **215**, 481–500 (2018).
4. Wilharm, A. et al. Mutual interplay between IL-17-producing gammadeltaT cells and microbiota orchestrates oral mucosal homeostasis. *Proc. Natl. Acad. Sci. USA* **116**, 2652–2661 (2019).
5. Maruyama, C. L., Monroe, M. M., Hunt, J. P., Buchmann, L. & Baker, O. J. Comparing human and mouse salivary glands: A practice guide for salivary researchers. *Oral. Dis.* **25**, 403–415 (2019).
6. Marsh, P. D., Do, T., Beighton, D. & Devine, D. A. Influence of saliva on the oral microbiota. *Periodontology 2000* **70**, 80–92 (2016).
7. Schenkels, L. C., Veerman, E. C. & Nieuw Amerongen, A. V. Biochemical composition of human saliva in relation to other mucosal fluids. *Crit. Rev. Oral. Biol. Med.* **6**, 161–175 (1995).
8. Tenovuo, J. Antimicrobial function of human saliva-how important is it for oral health? *Acta Odontol. Scand.* **56**, 250–256 (1998).
9. Brandtzaeg, P., Nilssen, D. E., Rognum, T. O. & Thrane, P. S. Ontogeny of the mucosal immune system and IgA deficiency. *Gastroenterol. Clin. North Am.* **20**, 397–439 (1991).
10. Zubeidat, K. et al. Microbiota-dependent and -independent postnatal development of salivary immunity. *Cell Rep.* **42**, 111981 (2023).
11. Jaber, Y. et al. Langerhans cells shape postnatal oral homeostasis in a mechanical-force-dependent but microbiota and IL17-independent manner. *Nat. Commun.* **14**, 5628 (2023).
12. Lamm, M. E. Interaction of antigens and antibodies at mucosal surfaces. *Annu Rev. Microbiol.* **51**, 311–340 (1997).
13. Niewiesk, S. Maternal antibodies: clinical significance, mechanism of interference with immune responses, and possible vaccination strategies. *Front Immunol.* **5**, 446 (2014).

14. Koch, M. A. et al. Maternal IgG and IgA Antibodies Dampen Mucosal T Helper Cell Responses in Early Life. *Cell* **165**, 827–841 (2016).
15. Macpherson, A. J., McCoy, K. D., Johansen, F. E. & Brandtzaeg, P. The immune geography of IgA induction and function. *Mucosal. Immunol.* **1**, 11–22 (2008).
16. Sanidad, K. Z. et al. Maternal gut microbiome-induced IgG regulates neonatal gut microbiome and immunity. *Sci. Immunol.* **7**, eabh3816 (2022).
17. Gu, H., Zou, Y. R. & Rajewsky, K. Independent control of immunoglobulin switch recombination at individual switch regions evidenced through Cre-loxP-mediated gene targeting. *Cell* **73**, 1155–1164 (1993).
18. Zeng, M. Y. et al. Gut Microbiota-Induced Immunoglobulin G Controls Systemic Infection by Symbiotic Bacteria and Pathogens. *Immunity* **44**, 647–658 (2016).
19. Weckel, A. et al. Long-term tolerance to skin commensals is established neonatally through a specialized dendritic cell subgroup. *Immunity* **56**, 1239–1254.e1237 (2023).
20. Zheng, W. et al. Microbiota-targeted maternal antibodies protect neonates from enteric infection. *Nature* **577**, 543–548 (2020).
21. Dang, C. V. c-Myc target genes involved in cell growth, apoptosis, and metabolism. *Mol. Cell Biol.* **19**, 1–11 (1999).
22. Youssef, K. K. & Nieto, M. A. Epithelial-mesenchymal transition in tissue repair and degeneration. *Nat. Rev. Mol. Cell Biol.* **25**, 720–739 (2024).
23. Yu, D. et al. Myogenic differentiation of stem cells for skeletal muscle regeneration. *Stem Cells Int.* **2021**, 8884283 (2021).
24. Ghaben, A. L. & Scherer, P. E. Adipogenesis and metabolic health. *Nat. Rev. Mol. Cell Biol.* **20**, 242–258 (2019).
25. Pearce, E. L. & Pearce, E. J. Metabolic pathways in immune cell activation and quiescence. *Immunity* **38**, 633–643 (2013).
26. Floter, J., Kaymak, I. & Schulze, A. Regulation of metabolic activity by p53. *Metabolites* **7**, 21 (2017).
27. Liu, H. & Chen, Y. G. The interplay Between TGF-beta signaling and cell metabolism. *Front Cell Dev. Biol.* **10**, 846723 (2022).
28. Nandula, S. R. et al. Salivary gland hypofunction induced by activation of innate immunity is dependent on type I interferon signaling. *J. Oral. Pathol. Med.* **42**, 66–72 (2013).
29. Rogier, E. W. et al. Secretory antibodies in breast milk promote long-term intestinal homeostasis by regulating the gut microbiota and host gene expression. *Proc. Natl. Acad. Sci. USA* **111**, 3074–3079 (2014).
30. Shenoy, M. K. et al. Breast milk IgG engages the mouse neonatal immune system to instruct responses to gut antigens. *Science* **389**, eado5294 (2025).
31. Atyeo, C. & Alter, G. The multifaceted roles of breast milk antibodies. *Cell* **184**, 1486–1499 (2021).
32. Bournazos, S. & Ravetch, J. V. Diversification of IgG effector functions. *Int Immunol.* **29**, 303–310 (2017).
33. Lukac, J. et al. Phagocytic functions of salivary neutrophils in oral mucous membrane diseases. *J. Oral. Pathol. Med.* **32**, 271–274 (2003).
34. Boruchov, A. M. et al. Activating and inhibitory IgG Fc receptors on human DCs mediate opposing functions. *J. Clin. Invest.* **115**, 2914–2923 (2005).
35. Ohsaki, A. et al. Maternal IgG immune complexes induce food allergen-specific tolerance in offspring. *J. Exp. Med.* **215**, 91–113 (2018).
36. van Montfoort, N. et al. Fcgamma receptor IIb strongly regulates Fcgamma receptor-facilitated T cell activation by dendritic cells. *J. Immunol.* **189**, 92–101 (2012).
37. Bruhns, P. Properties of mouse and human IgG receptors and their contribution to disease models. *Blood* **119**, 5640–5649 (2012).
38. Anderson, C. F. & Mosser, D. M. Cutting edge: biasing immune responses by directing antigen to macrophage Fc gamma receptors. *J. Immunol.* **168**, 3697–3701 (2002).
39. Getahun, A. & Heyman, B. Studies on the mechanism by which antigen-specific IgG suppresses primary antibody responses: evidence for epitope masking and decreased localization of antigen in the spleen. *Scand. J. Immunol.* **70**, 277–287 (2009).
40. Kuo, W. T., Odenwald, M. A., Turner, J. R. & Zuo, L. Tight junction proteins occludin and ZO-1 as regulators of epithelial proliferation and survival. *Ann. N. Y Acad. Sci.* **1514**, 21–33 (2022).
41. Dutzan, N. et al. On-going mechanical damage from mastication drives homeostatic Th17 cell responses at the oral barrier. *Immunity* **46**, 133–147 (2017).
42. Radaic A. et al. Specific oral microbial differences in proteobacteria and bacteroidetes are associated with distinct sites when moving from healthy mucosa to oral Dysplasia-A microbiome and gene profiling study and focused review. *Microorganisms* **11**, 1–29 (2023).
43. Fine, D. H., Patil, A. G. & Velusamy, S. K. Aggregatibacter actinomycetemcomitans (Aa) Under the Radar: Myths and Misunderstandings of Aa and Its Role in Aggressive Periodontitis. *Front Immunol.* **10**, 728 (2019).
44. Bender, J. K. et al. Combined clinical, epidemiological, and genome-based analysis identified a nationwide outbreak of burkholderia cepacia complex infections caused by contaminated mouthwash solutions. *Open Forum Infect. Dis.* **9**, ofac114 (2022).
45. Li, Q., Zhou, F., Su, Z., Li, Y. & Li, J. Corynebacterium matruchotii: A confirmed calcifying bacterium with a potentially important role in the supragingival plaque. *Front. Microbiol.* **13**, 940643 (2022).
46. Gross, K. et al. Simultaneous presence of Mycoplasma salivarium and Tannerella forsythia in the implant sulcus after lateral augmentation with autogenous root grafts is associated with increased sulcus probing depth. *PLoS One* **17**, e0270962 (2022).
47. Newman, M. G., Saglie, R., Carranza, F. A. Jr. & Kaufman, A. K. Mycoplasma in periodontal disease. Isolation in juvenile periodontitis. *J. Periodontol.* **55**, 574–580 (1984).
48. Sharma, N., Bhatia, S., Sodhi, A. S. & Batra, N. Oral microbiome and health. *AIMS Microbiol.* **4**, 42–66 (2018).
49. Jiao, Y. et al. Induction of bone loss by pathobiont-mediated Nod1 signaling in the oral cavity. *Cell Host Microbe* **13**, 595–601 (2013).
50. Han, Y. et al. Pasteurella multocida Toxin Aggravates Ligatured-Induced Periodontal Bone Loss and Inflammation via NOD-Like Receptor Protein 3 Inflammasome. *Cell. Microbiol.* **1**, 1–16 (2022).
51. Moutsopoulos, N. M. et al. Defective neutrophil recruitment in leukocyte adhesion deficiency type I disease causes local IL-17-driven inflammatory bone loss. *Sci. Transl. Med.* **6**, 229ra240 (2014).
52. de Paula, FMS., Herzberg, M. C., Masopust, D. & Stolley, M. J. Oral mucosa resident CD8 +T cell reactivation exacerbates murine periodontitis. *J. Immunol.* **18**, 620–630 (2023).
53. Conti, M. G. et al. Immune response of neonates born to mothers infected with SARS-CoV-2. *JAMA Netw. Open* **4**, e2132563 (2021).
54. Selner, J. C., Merrill, D. A. & Claman, H. N. Salivary immunoglobulin and albumin: development during the newborn period. *J. Pediatr.* **72**, 685–689 (1968).
55. Wan, A. K. et al. Immunoglobulins in saliva of preterm and full-term infants. *Oral. Microbiol. Immunol.* **18**, 72–78 (2003).
56. Caballero-Flores, G. et al. Maternal immunization confers protection to the offspring against an attaching and effacing pathogen through delivery of IgG in Breast Milk. *Cell Host Microbe* **25**, 313323 e314 (2019).
57. Vazquez-Pagan, A. et al. Maternal immunization with distinct influenza vaccine platforms elicits unique antibody profiles that impact the protection of offspring. *bioRxiv*, 1–49 https://doi.org/10.1101/2023.10.30.564827 (2023).

58. Bouxsein, M. L. et al. Guidelines for assessment of bone microstructure in rodents using micro-computed tomography. *J. Bone Min. Res.* **25**, 1468–1486 (2010).
59. Marcel, M. Cutadapt removes adapter sequences from high-throughput sequencing reads. *EMBnetjournal* **17**, 10–12 (2011).
60. Kim, D. et al. TopHat2: accurate alignment of transcriptomes in the presence of insertions, deletions and gene fusions. *Genome Biol.* **14**, R36 (2013).
61. Anders, S., Pyl, P. T. & Huber, W. HTSeq-a Python framework to work with high-throughput sequencing data. *Bioinformatics* **31**, 166–169 (2015).
62. Love, M. I., Huber, W. & Anders, S. Moderated estimation of fold change and dispersion for RNA-seq data with DESeq2. *Genome Biol.* **15**, 550 (2014).
63. Subramanian, A. et al. Gene set enrichment analysis: a knowledge-based approach for interpreting genome-wide expression profiles. *Proc. Natl. Acad. Sci. USA* **102**, 15545–15550 (2005).

Acknowledgements

We thank Prof. Gilad Bacrahch for the critical discussion of this manuscript. Funding: This work was supported by Israel Science Foundation Grant 404/25 (A-H.H).

Author contributions

Conceptualization: R.N., and A-H.H. Methodology: R.N., Y.A., Y.N., Y.J., S.Y., O.S., O.G., P.K., N.D., R.B., A.H., and L.E-B. Visualization: R.N. Funding acquisition: A-H.H, A.W. Contribution of germ-free mice: H.S. and E.E. Writing: A-H.H.

Competing interests

The authors declare no competing interests.

Additional information

Supplementary information The online version contains supplementary material available at https://doi.org/10.1038/s41467-026-71704-5.

Correspondence and requests for materials should be addressed to Avi-Hai Hovav.

Peer review information *Nature Communications* thanks the anonymous reviewers for their contribution to the peer review of this work. A peer review file is available.